Can Barents Sea Ice Decline in Spring Enhance Summer Hot Drought Events over Northeastern China?

HUIXIN LI

Nansen-Zhu International Research Centre, Institute of Atmospheric Physics, Chinese Academy of Sciences, and University of Chinese Academy of Sciences, Beijing, China

HUOPO CHEN, HUIJUN WANG, JIANQI SUN, AND JIEHUA MA

Nansen-Zhu International Research Centre, Institute of Atmospheric Physics, Chinese Academy of Sciences, Beijing, and Collaborative Innovation Center on Forecast and Evaluation of Meteorological Disasters, Nanjing University for Information Science and Technology, Nanjing, China

(Manuscript received 26 June 2017, in final form 6 March 2018)

ABSTRACT

In July–August (JA) of 2016, northeastern China (NEC) suffered from the most severe hot drought event of the past 50 years, leading to profound impacts on agriculture, the ecosystem, and society. Results indicate that the loss of sea ice over the Barents Sea (SICBS) in March might have influenced the hot drought events over NEC in JA for the period of 1997–2016. Further analyses reveal that lower SICBS is closely related to thinner snow depth over western Eurasia (SDWEA) in April. The decline of SDWEA leads to drier soil from the Yangtze River valley to northern China during May–June, which is favorable for precipitation deficiency over NEC in JA. Besides, the loss of SICBS in March and decline of SDWEA in April are closely related to the polar–Eurasia teleconnection pattern and dry soil over NEC in JA, which provides favorable atmospheric circulation patterns for occurrences of hot droughts. The large ensemble simulations from the Community Earth System Model and the numerical experiments based on version 4 of the Community Atmosphere Model further confirmed their connections and the associated possible physical processes. Therefore, snow depth and soil moisture might serve as linkages between Barents Sea ice in March and hot droughts over NEC during JA, and the Barents Sea ice in March might be an important potential predictor for the summer hot droughts over NEC.

1. Introduction

Drought is a major natural hazard that is often characterized by high temperature and below normal precipitation over a long period of time. As global warming intensifies, hot events occur more frequently, which further increases drought severity in many areas (Wang et al. 2012; Trenberth et al. 2014; Wang et al. 2016). In 2016, northeastern China (NEC) suffered a severe hot drought event during July–August (JA), resulting in a serious decrease in crop production with subsequent economic losses reaching CNY15.61 billion, according to official statistics. Since NEC is the granary of China, improving the understanding of drought occurrences and providing a usefully early warning are urgently important for both the government and the public.

Recently, China suffered from several prolonged severe drought disasters. In 2006, a severe drought event occurred over southeastern China with long rainless periods during summer (Li et al. 2011). During the winter season of 2009/10, southwestern China experienced its most severe drought event in the past 50 years (Yang et al. 2012), and the negative phase of the Arctic Oscillation and the ENSO event partially accounted for this drought. In summer 2014, the most severe drought event in the past 60 years occurred over northern China, mainly as the result of the joint effects of atmospheric, oceanic, and terrestrial anomalies (Wang and He 2015; Xu et al. 2017). From these studies, droughts were

Supplemental information related to this paper is available at the Journals Online website: https://doi.org/10.1175/JCLI-D-17-0429.s1.

Corresponding author: Chen Huopo, chenhuopo@mail.iap.ac.cn

DOI: 10.1175/JCLI-D-17-0429.1

© 2018 American Meteorological Society. For information regarding reuse of this content and general copyright information, consult the AMS Copyright Policy (www.ametsoc.org/PUBSReuseLicenses).

Unauthenticated | Downloaded 08/04/22 06:29 PM UTC

usually defined as the negative precipitation condition, and the effect of temperature anomalies was generally neglected. However, the role of temperature anomaly with regard to drought occurrence has become more and more important, especially under the background of global warming (Chen and Sun 2015a,b).

Prior to the current study, numerous studies have focused on the variations and physical mechanisms relating to precipitation anomalies over NEC. Generally, summer precipitation over NEC exhibited a decreasing trend during the past half century (Liang et al. 2011), which potentially increased the probability of occurrences of drought events (Zhang et al. 2013). In terms of the decadal variations, Han et al. (2015) found that NEC has experienced a decadal decrease in the late 1990s, and the shift of the Pacific decadal oscillation (PDO) and changes in the Arctic sea ice concentration accounted for this change. Besides, other studies suggested that the East Asian summer monsoon (EASM) also accounted for the decadal variations of precipitation over eastern China (Wang 2001; Ding et al. 2009). For the causal factors of the interannual variations, some studies indicated that the EASM (Sun et al. 2007, 2017) and the North Atlantic Oscillation (NAO) are highly correlated with summer precipitation over NEC (Sun and Wang 2012). Additionally, the global sea surface temperature distribution and the preceding ENSO event also presents a close relationship with summer precipitation over NEC (Sun et al. 2004; Han et al. 2017).

Severe drought events have become more frequent in NEC in recent decades (Yu et al. 2014; Liu et al. 2015; Chen and Sun 2017a) and the anthropogenic warming might partly account for this change (Chen and Sun 2017b). Some studies have focused on the effects of the ENSO event (Dai 2013; X. Li et al. 2015) and winter NAO (Fu and Zeng 2005) on interannual variations in summer drought events over NEC, but few have considered the effects of sea ice concentration (SIC). In recent years, the role of sea ice has been gradually debated and acknowledged for its influence on global climate changes (Liu et al. 2012; Screen et al. 2013, 2014; Gao et al. 2015; Kelleher and Screen 2017). Some studies also found that the decline of Arctic sea ice in recent decades presents significant effects on the climate across China (Li and Wang 2013; Guo et al. 2014; Wang and He 2015; Wang et al. 2015; Wang and Chen 2016).

In particular, the variations during autumn–winter SIC over the Barents Sea have great impacts on climate over midlatitudes of Northern Hemisphere (Petoukhov and Semenov 2010; Inoue et al. 2012; Kim et al. 2014) and can further influence temperature anomalies (F. Li et al. 2015), the winter monsoon (Wu et al. 1999), and dust events (Fan et al. 2018) over China. Recently, He et al. (2018) found that the reduction of sea ice over the Barents Sea in June excites an anomalous Silk Road pattern, which leads to an anomalous precipitation pattern over East Asia. However, there is still a continuing debate as to whether recent Arctic sea ice loss has significantly influenced the midlatitude weather (Barnes and Screen 2015), and some studies have turned to large ensemble models to see whether those correlations just reflect the atmospheric internal variability (e.g., Seviour 2017). Besides, few studies have investigated the possible linkages between spring Barents Sea ice and summer climate changes over China. Therefore, variations of SIC over the Barents Sea region in spring will be investigated and examined in terms of possible connections to the summer hot droughts over NEC, which might provide useful information for the prediction and understanding of summer hot droughts over NEC.

First, we investigate drought events concerning the concept of the return period in a multivariate framework. Generally, the return period provides important information to assess risks of climate extreme events. To identify the return period of the concurrent climatic events, multivariate copula methods were developed and then widely used worldwide (De Michele et al. 2005; Salvadori and De Michele 2010; Zhang et al. 2013). Recently, a new multivariate approach based on survival copulas and the relevant survival Kendall's measurement was further developed by Salvadori et al. (2013), where the safe region of the extreme event is bounded. Based on this method, the severe drought event over California in 2014 has been well described (AghaKouchak et al. 2014; Cheng et al. 2016). However, few studies have applied this method to analyze hot drought events over China, which forms the topic of this study. Since more work is needed regarding this aspect, we investigate the associated atmospheric circulations and its possible physical mechanisms relating to summer hot drought events over NEC based on this multivariate survival method. The joint survival cumulative distribution function is calculated here to assess the risks of hot droughts by simultaneously considering the precipitation deficiency and high-temperature anomalies.

The outline of this study is as follows. Section 2 gives a simple introduction to datasets used in this research. Section 3 describes the analysis methods concerning the joint survival approach. Section 4 describes the concurrent hot drought event over NEC in 2016 and the atmospheric circulation anomalies for hot drought events over NEC, and then the related possible physical

Unauthenticated | Downloaded 08/04/22 06:29 PM UTC

mechanisms are further discussed and verified. A brief summary and discussion are presented in section 5.

2. Data

a. Observational and reanalysis datasets

Observational daily precipitation and temperature datasets during 1960–2016 are collected from the National Meteorological Information Center of China Meteorological Administration, with 78 stations available in NEC (within 42°–54°N, 110°–135°E). These datasets are interpolated onto 1° × 1° grids using the iterative improvement objective method provided by the NCAR Command Language. In addition, monthly reanalysis datasets derived from the National Centers for Environmental Prediction (NCEP)–National Center for Atmospheric Research (NCAR) data with a horizontal resolution of 2.5° × 2.5° (Kalnay et al. 1996) are employed in this study. Variables including surface pressure, meridional and zonal winds, vertical velocity, geopotential height, surface air temperature (SAT), and specific humidity are used here. Monthly Arctic SIC datasets are obtained from the Hadley Centre Sea Ice and SST dataset, version 1 (HadISST1), with a resolution of 1° × 1° (Rayner et al. 2003). Monthly mean snow depth datasets derived from the ERA-Interim land data with a resolution of 1° × 1° are also employed (Balsamo et al. 2015). Monthly reanalysis datasets of soil moisture from ERA-Interim with a resolution of 1.0° × 1.0° are obtained, and we focus on the top layer of soil moisture. The polar–Eurasian teleconnection pattern (POL) index that is defined by the Climate Prediction Center as a mode of geopotential height at 700 hPa and provided by NOAA (available online at http://www.cpc.ncep.noaa.gov/data/teledoc/telecontents.shtml) is also employed. The Atlantic multidecadal oscillation (AMO) index is derived from the Earth System Research Laboratory (available online at https://www.esrl.noaa.gov/psd/data/correlation/amon.us.data).

In our study, the PINEC index is defined as the spatially weighted probability-based index (PI) over NEC (within 42°–54°N, 110°–135°E). The SICBS index is calculated as the spatially weighted SIC averaged over the Barents Sea (within 72°–77°N, 30°–60°E). The SDWEA index is defined as the spatially weighted snow depth averaged over western Eurasia (within 55°–70°N, 30°–60°E). The SMNEC index is defined as the spatially weighted soil moisture averaged over NEC (within 42°–54°N, 110°–135°E).

b. Community Earth System Model Large Ensemble datasets

To provide evidence that supports the proposed connections between sea ice/snow cover and hot drought events over NEC, the simulations from the Community Earth System Model Large Ensemble (CESM-LE) datasets are employed (Kay et al. 2015). There are 35-member ensembles included in CESM-LE, with a horizontal resolution of 0.9° latitude × 1.25° longitude and 30 vertical levels. The CESM-LE is based on the Community Atmosphere Model version 5, which consists of coupled atmosphere, ocean, land, and sea ice component models. Here, the simulated monthly historical forcing (1920–2005) and the future representative concentration pathway 8.5 (RCP8.5) forcing (2006–2100) datasets are employed. The variables used here include surface air temperature, precipitation, surface pressure, meridional and zonal winds, vertical velocity, geopotential height, sea ice fraction, snow depth, and soil moisture.

3. Method

The univariate return period of a certain extreme event is calculated as

$$R(x) = \frac{1}{\omega[1 - F(x)]}, \tag{1}$$

where $R(x)$ is the return period, $\omega = 1\ \mathrm{yr}^{-1}$ is the average sampling frequency, and $F(x)$ is the cumulative distribution function (CDF) value (Wilks 2011).

The covariate return period of an extreme event is related to the concept of multivariate copula. In our study two variables, x_1 (precipitation) and x_2 (temperature), are considered simultaneously, where $F_1(x_1) = P(X_1 \le x_1)$ and $F_2(x_2) = P(X_2 \le x_2)$ are the associated CDFs. According to previous definitions, the joint CDF is calculated as $F(x_1, x_2) = C[F_1(x_1), F_2(x_2)]$ (Salvadori et al. 2011). To identify dangerous regions, the concept of a joint survival function (e.g., t copula, Gaussian copula, and Gumbel copula) is employed (Salvadori et al. 2013), and the survival CDF is calculated as $\overline{F}_i = 1 - F_i$. Specifically, we use the PI to represent the joint survival CDF, which is shown by

$$\mathrm{PI} = \hat{C}[\overline{F}_1(x_1), \overline{F}_2(x_2)] = P(X_1 > x_1, X_2 > x_2). \tag{2}$$

Thus, given a probability level of t, the corresponding survival layer $L_t^{\overline{F}}$ is obtained as $L_t^{\overline{F}} = \{x \in R^d : \overline{F}(x) = t\}$. Apparently, for any $x \in R^d$, there exists a unique marginal survival layer to meet the criterion function of $\overline{F}(x) = t$ (Salvadori et al. 2011). According to these definitions, the survival Kendall's return period $\overline{\kappa}_x$ is defined as

$$\overline{\kappa}_x = \frac{\mu}{1 - \overline{K}(t)}, \tag{3}$$

Unauthenticated | Downloaded 08/04/22 06:29 PM UTC

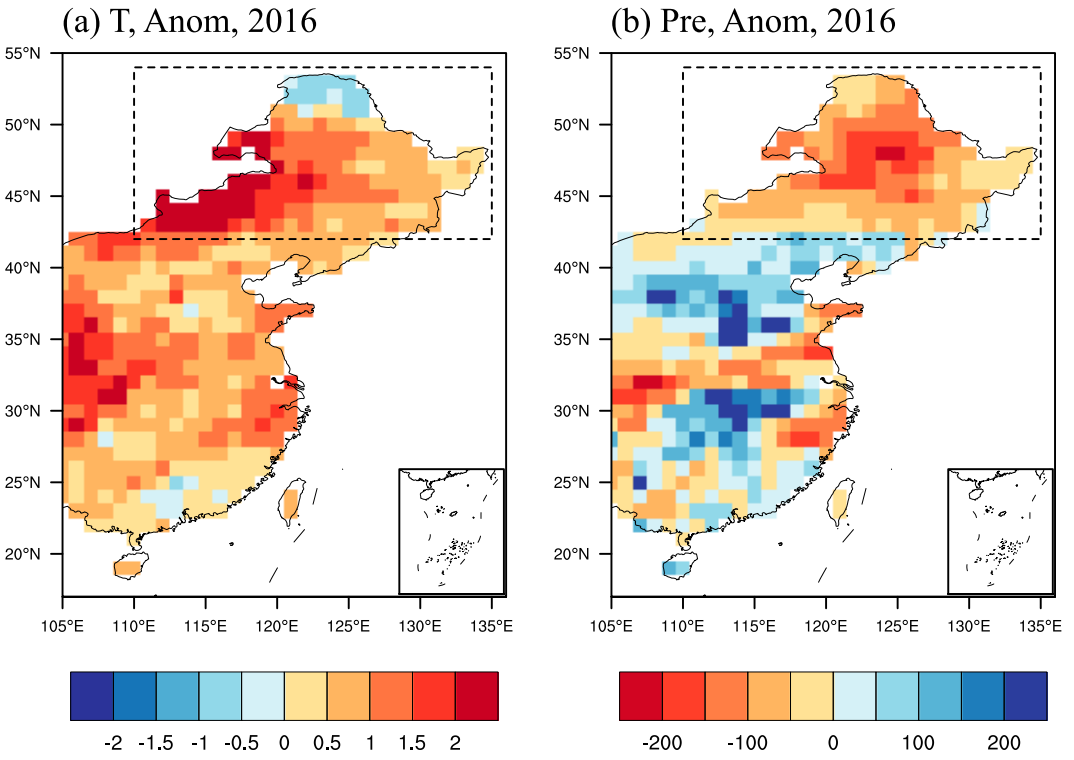

FIG. 1. Spatial distribution of (a) temperature (°C) and (b) precipitation (mm) anomalies during JA in 2016 relative to the climatology of 1981–2010.

where μ is the recurrence interval (Salvadori et al. 2013), and $\overline{K}(t)$ is the survival function associated with $\overline{F}(x)$ defined as

$$\overline{K}(t) = P[\overline{F}(X_1, X_2) \geq t] = P\{\hat{C}[\overline{F}_1(x_1), \overline{F}_2(x_2)] \geq t\}. \quad (4)$$

For a certain return period T, the probability level p is given by $p = 1 - \mu/T$, and the survival Kendall's quantile of order $\overline{q}$ is calculated according to the following equation:

$$\overline{q} = \overline{q}(p) = \sup\{t \in I : \overline{K}(t) = p\} = \overline{K}^{(-1)}(p). \quad (5)$$

Consequently, the survival Kendall's layer $L_t^{\overline{F}}$ provides the set of conditions that share a joint return period when $\overline{q}$ is given.

4. Results

a. *Hot droughts in JA 2016 over NEC*

Figure 1 shows the spatial patterns of the anomalous temperature and precipitation during JA in 2016 with respect to the climatology of 1981–2010. Clearly, there was a strong positive temperature center (Fig. 1a) and a considerable negative precipitation center (Fig. 1b) over NEC, indicating the concurrence of strong precipitation deficiency and a high-temperature event in 2016. To understand the general variability of temperature and precipitation over NEC, we calculate the relevant area-weighted temporal series (Fig. 2). It is clear that the temperature in 2016 was the second highest year during 1960–2016, following the year of 2000 (Fig. 2, top). In terms of precipitation deficit, drought in 2016 over NEC was the second most severe year during 1960–2016 (Fig. 2, middle), and the year of 2007 was the most severe drought year in the historical record (during 1960–2016).

For univariate climatic events, the recurrence interval of precipitation deficiency in 2016 was estimated to be 34 yr, and it was estimated to be 16 yr for high temperature based on the univariate method in Eq. (1). Clearly, estimation for the risk of a drought event in 2016 varies when considering different univariate climatic information. In fact, extreme precipitation deficiency and high temperature events do not necessarily occur at the same time, but the concurrence of an extreme event with another event might induce much stronger extreme events (AghaKouchak et al. 2014). Thus, the multivariate framework is employed to identify risk of the strong precipitation deficiency and high temperature event over NEC in JA 2016 [see Eqs. (2)–(5)]. Figure S1 in the supplemental material presents the return period distribution of hot droughts over NEC during 1960–2016

Unauthenticated | Downloaded 08/04/22 06:29 PM UTC

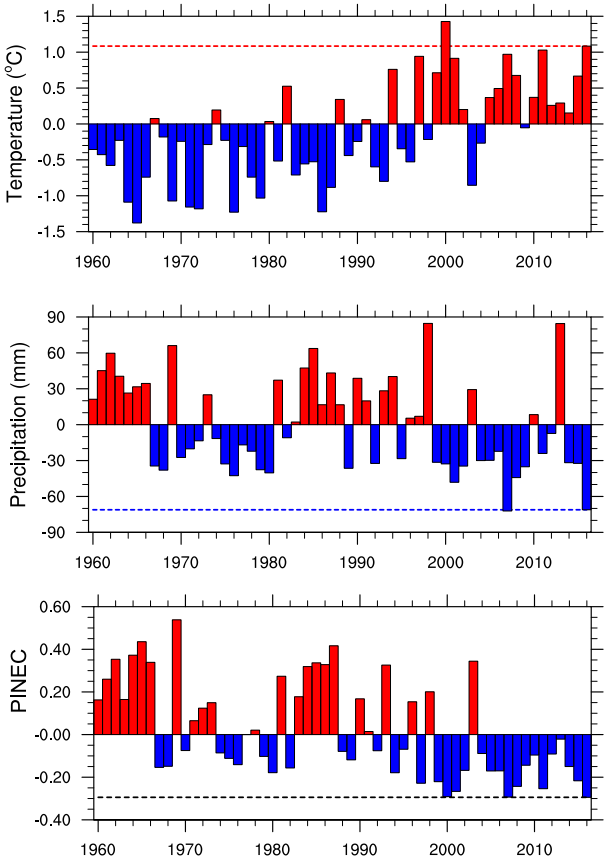

FIG. 2. Time series of area-weighted anomalies over NEC in JA relative to the climatology of 1981–2010 in (top) temperature, (middle) precipitation, and (bottom) PINEC (spatially weighted, averaged over 42°–54°N, 110°–135°E) concerning the joint survival cumulative distribution of precipitation deficiency and high temperature. The dotted lines represent the corresponding anomalous levels in 2016.

using t copula survival methods described in section 3, which is a good fit at the 95% confidence level with an acceptable p value of 0.66. Similar results can be obtained from the Gaussian copula and Gumbel copula methods (Durante and Salvadori 2010; Salvadori and De Michele 2010). We can find that the drought in JA 2016 has been up to a high level and has broken the historical record in the past 50 years when the temperature and precipitation anomalies are considered simultaneously. This drought event is estimated to occur once in approximately 40 years. However, if we only consider the univariate climatic factor for this drought event in JA 2016, the occurrence probability is generally overestimated. The return period is estimated to be 34 yr when only precipitation is considered. Thus, high temperature over NEC increased the severity of drought in 2016. The most severe drought event in NEC occurred in 2016 during the period 1960–2016 and was the joint result of precipitation deficiency and high temperature; the drought during JA in 2007 was the second most severe, and the drought during JA in 2000 was the third most severe.

Results indicate that the univariate risk estimation might underestimate (e.g., drought in 2016) or overestimate (e.g., drought in 2007) the risk of extreme events. However, multivariate survival methods are more reliable and can provide valuable information for decision-making (AghaKouchak et al. 2014). Therefore, the PI concerning the joint survival cumulative distribution of precipitation deficit and high temperature [see Eq. (2)] is further analyzed. Figure 2, bottom, shows the area-weighted temporal series of PI anomalies during 1960–2016 over NEC (PINEC). Clearly, variations of PINEC present similarities with the precipitation series, while high temperature generally exacerbates the drought events that result in lower PINEC values (e.g., drought in 2016). Typically, the PINEC value represents the probability of the concurrent hot drought event over NEC in JA, and a lower value represents a stronger, hotter drought event. Hence, the lowest value in 2016 suggests that NEC suffered the most severe hot drought event during JA, also supporting the results from Fig. S1.

b. *Anomalous atmospheric patterns for the hot droughts over NEC*

To document the atmospheric circulation patterns relevant to hot drought events in NEC, regression maps of the atmospheric circulation patterns in JA against PINEC during 1960–2016 are illustrated in Fig. 3. To facilitate comparisons in the following analyses, we multiply −1 by PINEC in this case. Here, wind anomalies and water vapor transport that associated with PINEC are first examined. Clearly, there is a significant anomalous anticyclonic system located over northern Asia from 200 (Fig. 3a) to 850 hPa (Fig. 3b), along with an apparent anomalous anticyclonic integrated water vapor transport (WVT; integrated from the surface to 300 hPa) (Fig. 3c). These anticyclonic anomalies of wind and WVT are unfavorable for the accumulation of moisture, thus playing an essential role in the induction of a precipitation deficiency over NEC. Furthermore, there exists a well-organized tripole pattern of geopotential height at 500 hPa with a significant positive center over NEC and two negative centers to the northwest and southeast (Fig. 3d), which well resembles the positive POL pattern. Similar patterns are also found at 200 and 850 hPa (figures not shown), indicating a quasi-barotropic effect. Therefore, the coherent positive anomalous geopotential height center from 850 to 200 hPa favors high temperature, thus strengthening the severity of the drought event over NEC. The regression results

Unauthenticated | Downloaded 08/04/22 06:29 PM UTC

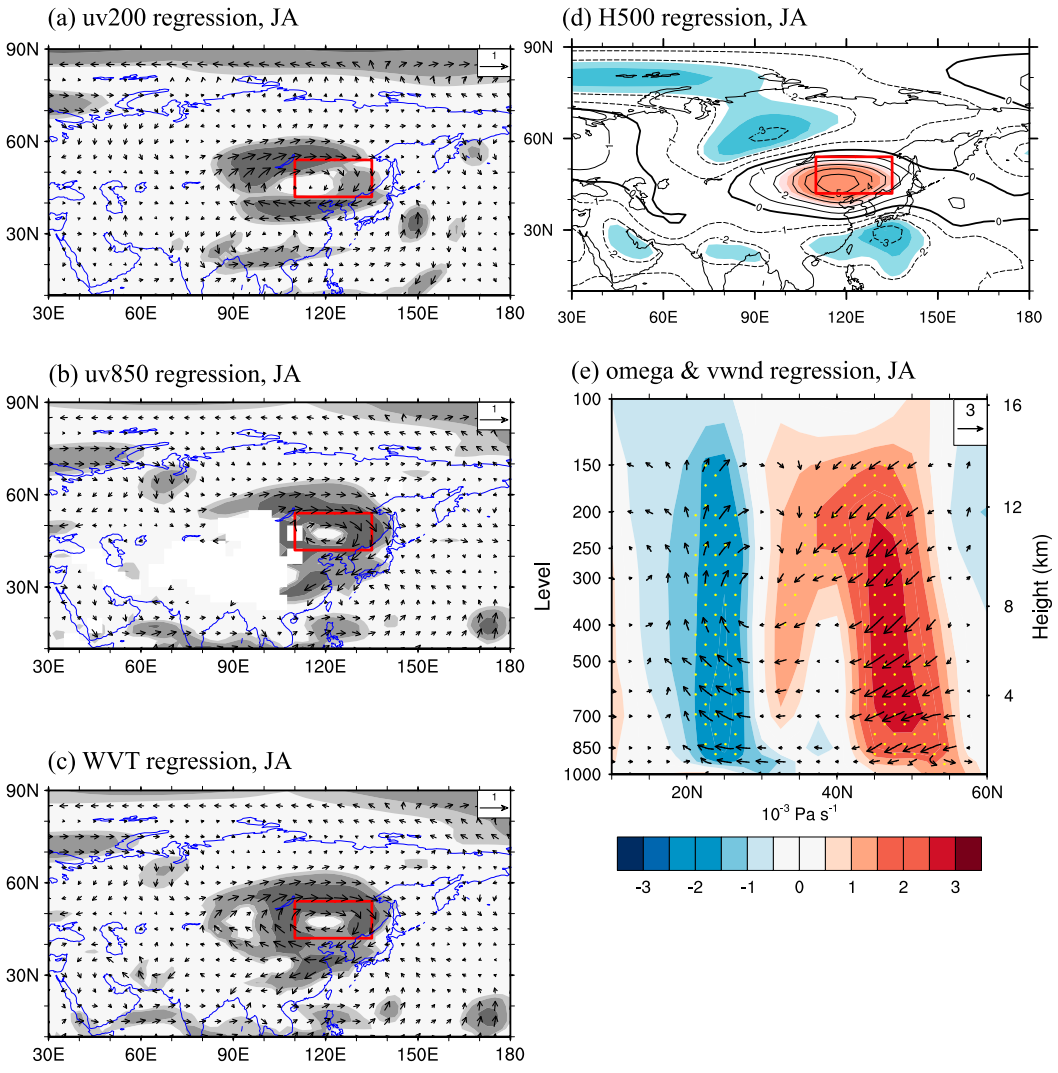

FIG. 3. Regression maps of the circulations in JA with regard to PINEC during 1960–2016, based on detrended and standardized series: (a) 200- and (b) 850-hPa wind, (c) integrated water vapor transport, (d) 500-hPa geopotential height, and (e) vertical–horizontal cross section averaged along 115°–135°E for vertical wind. Shading from light to dark in (a)–(d) indicate the regression coefficient significant at the 90%, 95%, and 99% confidence levels based on the Student's *t* test. The color shading in (e) indicates vertical velocity ω anomalies, and the dotted regions indicate the regression coefficient significant at the 90% confidence level based on the Student's *t* test. Here, PINEC is multiplied by −1.

of vertical motions against PI indicate that drought over NEC is accompanied by a significant, uniform downward vertical motion over NEC (about 42°–55°N), along with significant, uniform upward vertical motion over eastern–southern China (about 20°–30°N). Clearly, the downward motion favors adiabatic heating over NEC (Fig. 3e).

For the severe hot drought event in 2016, the corresponding atmospheric circulation anomalies (relative to the climatology of 1981–2010) are shown in Fig. 4. Obviously, the anomalous anticyclonic wind (Figs. 4a,b) and WVT (Fig. 4c) centers are evident over northern Asia, indicating the stronger-than-normal northerly flow in NEC, opposite to the climatologically typical southwesterly. Thus, less water vapor was transported to this region, leading to precipitation deficiency in 2016. Furthermore, the anomalous positive geopotential height over northern Asia at 500 hPa (Fig. 4d) was also consistent with the regression results in Fig. 3d, and the anomalous descending motion over NEC (Fig. 4e) was similar to the regression pattern in Fig. 3e, and both phenomena contributed to the higher temperature over NEC. These anomalous atmospheric circulations in 2016 were in good agreement with the regression results

Unauthenticated | Downloaded 08/04/22 06:29 PM UTC

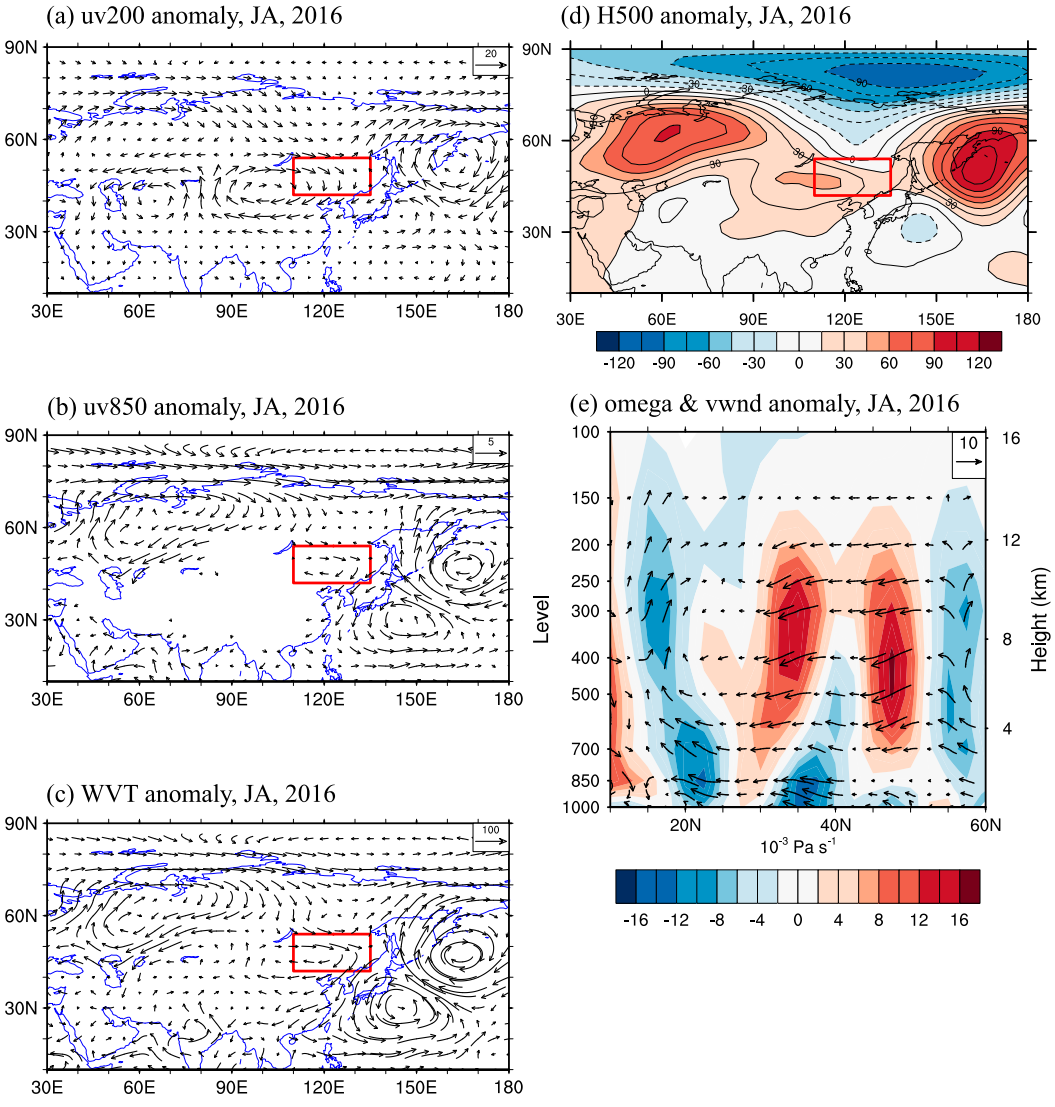

FIG. 4. The circulation anomalies during JA in 2016 (relative to the climatology of 1981–2010) for (a) 200- and (b) 850-hPa wind (m s^{-1}), (c) integrated water vapor transport (kg m^{-1} s^{-1}), (d) 500-hPa geopotential height (gpm), and (e) vertical–horizontal cross section averaged along 115°–135°E for vertical wind. The color shading in (e) indicates ω anomalies (10^{-3} Pa s^{-1}).

against PI, and they created a favorable environment for less precipitation and higher temperature over NEC.

Gao et al. (2017) suggested that the POL teleconnections could influence atmospheric circulations over the Eurasia, and the above analyses have implied that the regressed geopotential height against PINEC shows similarity to the positive POL pattern in summer. Here, POL series that derived from NOAA are employed to investigate the temporal relationship between PINEC and POL indices in the past decades. The interannual variation of POL and PINEC are substantially consistent, with strong negative correlation coefficient of −0.51 for the standardized series and −0.37 for the detrended series, both of which are significant at the 99% confidence level based on the Student's t test. Moreover, the anomalous POL value in JA 2016 was one of the largest during 1960–2016 (Fig. S2 in the supplemental material), corresponding to the synchronous lowest PINEC value in 2016 (Fig. 2c). Figure 5 illustrates regression maps of the atmospheric circulations during JA in 1960–2016 against POL. Remarkably, the regressed atmospheric circulations onto POL index are reasonably similar to that of PINEC index. The presence of the POL pattern is clearly proven by the regressed geopotential height fields. As a result, the positive POL pattern favors anomalous high geopotential height over

Unauthenticated | Downloaded 08/04/22 06:29 PM UTC

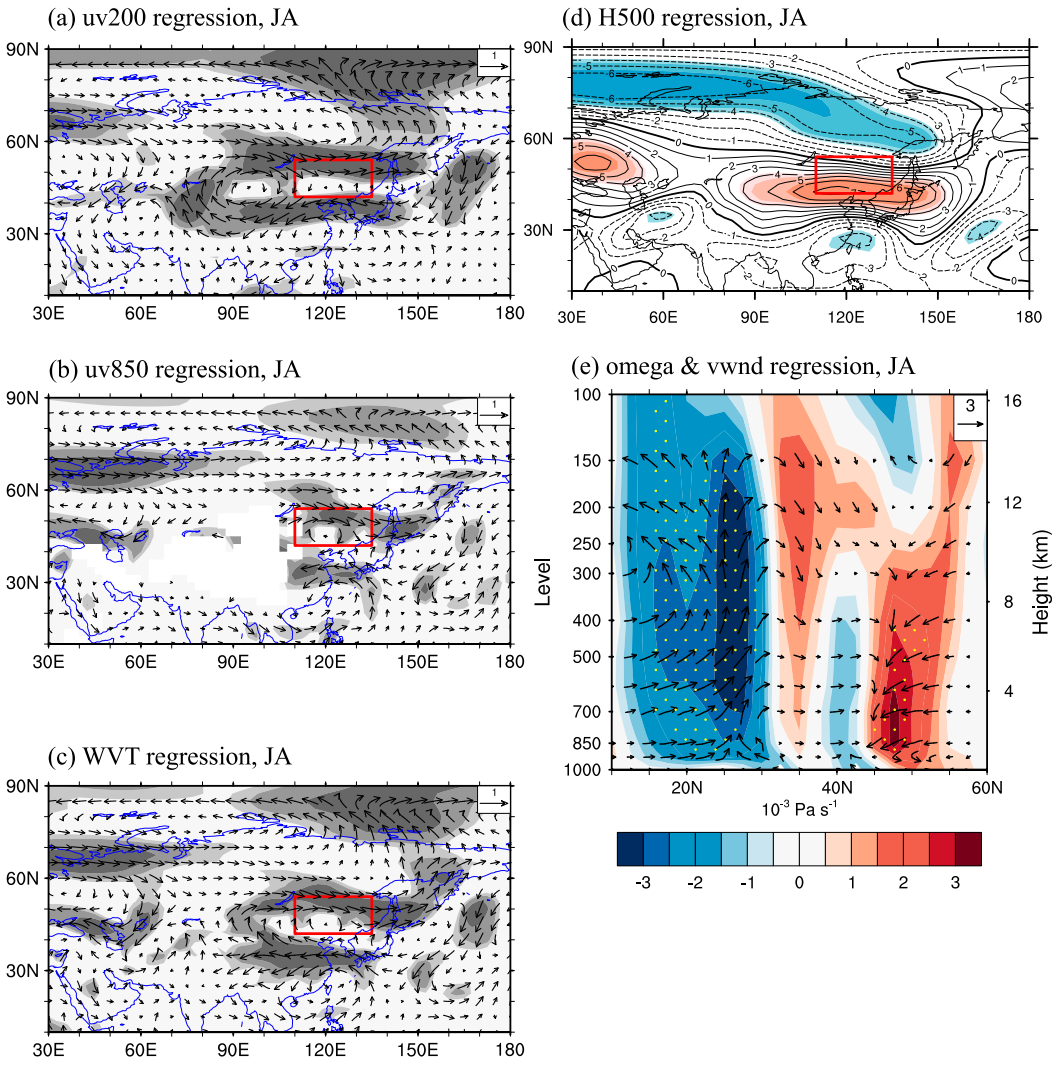

FIG. 5. As in Fig. 3, but for the regression maps of atmospheric circulations with regard to the POL during JA.

North Asia (Fig. 5d), which further induces downward motion (Fig. 5e) along with the anomalous northerly flow (Figs. 5a–c) over NEC, thus inducing insufficient moisture concentration and high temperature. Thus, positive POL pattern is closely connected to drought-relevant atmospheric circulation anomalies, and the stronger-than-normal POL index in 2016 (Fig. S2) was favorable for the occurrence of that severest hot drought event.

c. *Impacts of Barents Sea ice on the hot drought occurrence over NEC*

The atmospheric circulation anomalies have been discussed for the hot drought events over NEC in the previous sections. In the following, the possible causal factors of these anomalous circulation patterns are further investigated, which can improve our understanding of these types of events and provide valuable information for their prediction.

Previous studies have indicated that there is a close relationship between sea ice over the Barents Sea and the climates across China (Wu et al. 1999; Petoukhov and Semenov 2010; Inoue et al. 2012; Kim et al. 2014; Fan et al. 2018; He et al. 2018). Thus, the relationship between SIC and PINEC is first calculated. Figure 6 displays the time series of SICBS in March and PINEC in JA from 1979 to 2016. SICBS and PINEC exhibit obvious interannual variability during 1979–2016, and their variations are more in phase after 1996/97 (Fig. 6a). The correlation coefficients between PINEC and SICBS are 0.41 for the entire period, −0.1 during 1979–96, and 0.75 during 1997–2016. Correlations during the entire

Unauthenticated | Downloaded 08/04/22 06:29 PM UTC

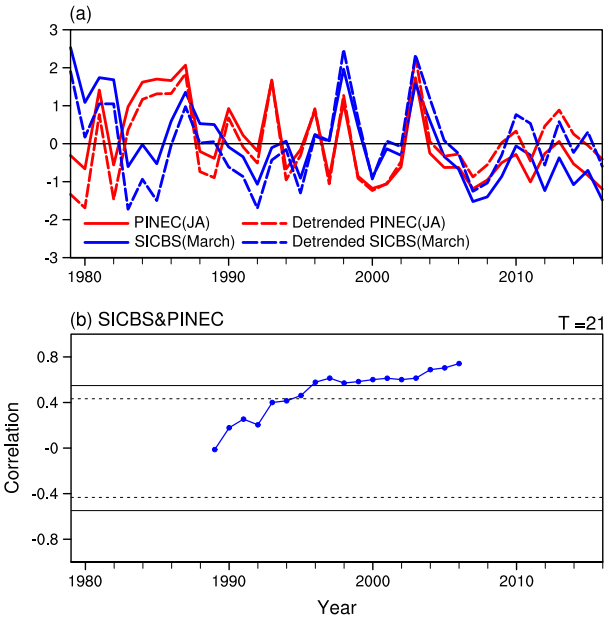

FIG. 6. (a) Time series of PINEC in JA (red) and SICBS (spatially weighted, averaged over 72°–77°N, 30°–60°E) in March (blue) during 1979–2016 for standardized (solid lines) and detrended series (dashed lines). (b) The 21-yr sliding correlation coefficient between PINEC and SICBS, based on the detrended series. The dashed (solid) horizontal lines represent correlations significant at the 95% (99%) confidence level based on Student's *t*-test.

period and the later period are significant at the 99% confidence level based on the Student's *t* test, and the correlation is even higher (0.82) during 1997–2016 when the linear trend is removed. Figure 6b shows the 21-yr sliding correlation coefficients between SICBS and PINEC, and their correlation increases significantly after the mid-1990s. Besides, the correlations between SICBS and SAT/precipitation over NEC are also given in Fig. S3 of the supplemental material, showing that both SAT and precipitation has very close relationship with SICBS during 1997–2016. The correlation is −0.70 (0.69) for SAT (precipitation) and SICBS; both are significant at the 99% confidence level based on the Student's *t* test.

Figures 7a and 7b show the regression maps of SIC in March with regard to PINEC in JA for two periods, respectivley. Clearly, SIC anomalies over the Barents Sea exhibit a strong positive relationship with PINEC during 1997–2016, whereas there is almost no significant regression coefficient over the Barents Sea during 1979–96. Similarly, we also focus on regression maps of the PI in JA with regard to SICBS in March. During 1997–2016, the PI over NEC is strongly correlated to SICBS, accompanied with widespread positive regression coefficients over NEC that are significant at the 95% confidence level based on the Student's *t* test (Fig. 7d). In contrast, only scattered positive coefficients appear in some parts of NEC during 1979–96 (Fig. 7c).

The aforementioned results show that the occurrences of hot droughts in JA over NEC might be linked to sea ice melting in March over the Barents Sea. A question would be thus raised as to how the SICBS in March exerts influence on the following summer hot drought events over NEC. Previous studies have suggested that SIC has a close relationship with snow depth (Li and Wang 2014) and snow cover (Fan et al. 2018), which can further influence the climate in China (Wu and Kirtman 2007; Wu et al. 2014; Zhang et al. 2016). We therefore focus on the regression maps of snow depth (SD) in April with regard to SICBS in March and PINEC in JA (Fig. 8). Clearly, snow depth over western Eurasia (WEA: within 55°–70°N, 30°–60°E) is highly correlated with SICBS in March (Fig. 8a), and this region also presents a positive relationship with PINEC in JA (Fig. 8b). In general, the reduction of SICBS in March could excite stationary Rossby waves (Fan et al. 2018) that would propagate southward and lead to anomalous adiabatic heating over WEA (Wu et al. 2011). Then, the warmer SAT over WEA in April (Fig. S4 in the supplemental material) would increase the rate of melting, leading to decreased snow depth over that region in April, which might be further linked to hot droughts over NEC according to Fig. 8b (the associated physical mechanisms will be explained in the following).

Here, we define the SDWEA as the area-averaged snow depth over WEA in April, and then calculate the 21-yr sliding correlation coefficients between SDWEA and SICBS (PINEC; Fig. 8c). The correlation between SDWEA and SICBS is very high during the entire period, significant at the 99% confidence level based on the Student's *t* test. In contrast, the relationship between SDWEA and PINEC was not obvious before the mid-1990s, but it increased significantly around 1996/97, which is consistent with the enhanced relationship between SICBS and PINEC after 1996/97. Time series of SDWEA and PINEC during 1997–2014 are plotted in Fig. 8d, with strong interannual relationship of 0.66 (0.71 for the detrended series) between them, significant at the 99% confidence level. These findings indicate that snow depth over WEA might play an important role linking the SICBS in March to the PINEC in JA.

Generally, soil moisture is an important indicator for drought events, which affects atmospheric circulations through evaporation–precipitation feedbacks and energy exchanges between the land and the atmosphere. Zhang and Zuo (2011) indicated that the influence can last for 2–3 months, and they found that the spring soil from the Yangtze River valley to northern China (YRNC: 30°–40°N, 105°–120°E) is significantly correlated with the

Unauthenticated | Downloaded 08/04/22 06:29 PM UTC

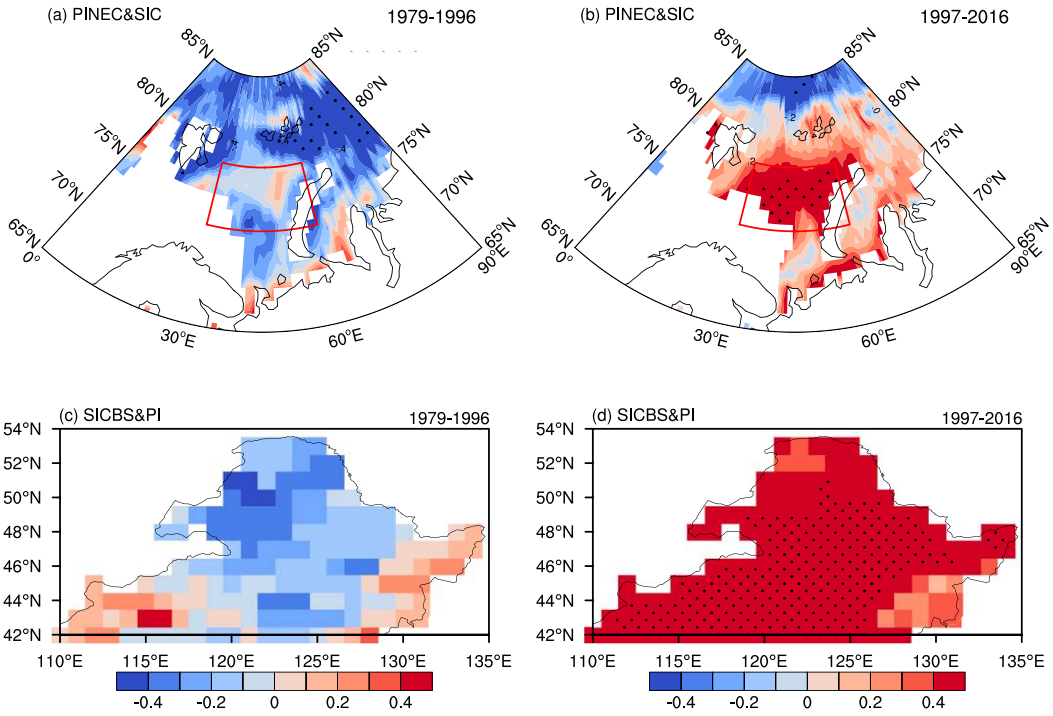

FIG. 7. Regression maps of the sea ice concentration in March with regard to PINEC during (a) 1979–96 and (b) 1997–2016. The red box indicates the Barents Sea (72°–77°N, 30°–60°E). Regression maps of PI in JA with regard to SICBS during (c) 1979–96 and (d) 1997–2016. Results are based on detrended and standardized series, and the dotted regions represent regression coefficient significant at the 95% confidence level based on the Student's *t* test.

summer precipitation over NEC. The abnormally dry soil over YRNC accounts for less evaporation, insufficient specific humidity, and higher SAT. Then the higher SAT over YRNC in May–June (MJ) is connected to less precipitation over NEC in JA by influencing EASM and summer atmospheric circulations. In addition to these persistent influences, Zhang and Zuo (2011) also found a dominant role of summer soil moisture in regulating summer precipitation and temperature over NEC. In fact, the dry SMNEC in JA also provides favorable atmospheric circulations for hot droughts over NEC in JA (see Fig. S5 in the supplemental material), inducing higher SAT (Fig. 9g), less precipitation (Fig. 9h), and hot drought event (Fig. 9i).

Thus, we further explore whether SICBS in March and SDWEA in April can influence soil moisture over YRNC in spring or SMNEC in JA, which are further linked to hot droughts over NEC in summer. Figure 10 shows the regression maps of soil moisture with respect to SICBS and SDWEA, and we multiply −1 by SICBS and SDWEA in this case. Clearly, the decrease of SDWEA in April leads to dry soil condition (Fig. 10c) over YRNC and over NEC in the following MJ, while the decline of SICBS in March present less significance than that of SDWEA (Fig. 10a). By contrast, both the decline of SICBS in March and the decrease of SDWEA in April favor dry conditions over NEC in JA (Figs. 10b,d). This result is consistent with Wu et al. (2014), whose work indicated that less summer precipitation and dry soil moisture over NEC correspond to less spring snow cover over the western Eurasian after 1990s. Therefore, soil moisture can serve as an important bridge linking SICBS/SDWEA and summer hot droughts over NEC.

Previous studies have proposed that variations of Arctic sea ice (Wu et al. 2013) and western snow cover (Wu et al. 2014) have a close relationship to atmospheric circulations in summer over Eurasia, and snow depth can influence the thermal conditions of land surface and atmospheric circulations by affecting albedo and hydrology (Barnett et al. 1989). The signal of the decreased SICBS in March can persist from spring to summer, thus resulting in decreased sea ice cover over the Barents–Kara Seas in JA (Fig. S6a in the supplemental material). Then the decreased SIC over the Barents–Kara Seas in JA may excite Rossby waves (He et al. 2018), which helps to form the POL-like pattern (Fig. S6b). Besides, the decrease of SIC over the Barents–Kara Seas in JA is accompanied with warm surface air temperature, which

Unauthenticated | Downloaded 08/04/22 06:29 PM UTC

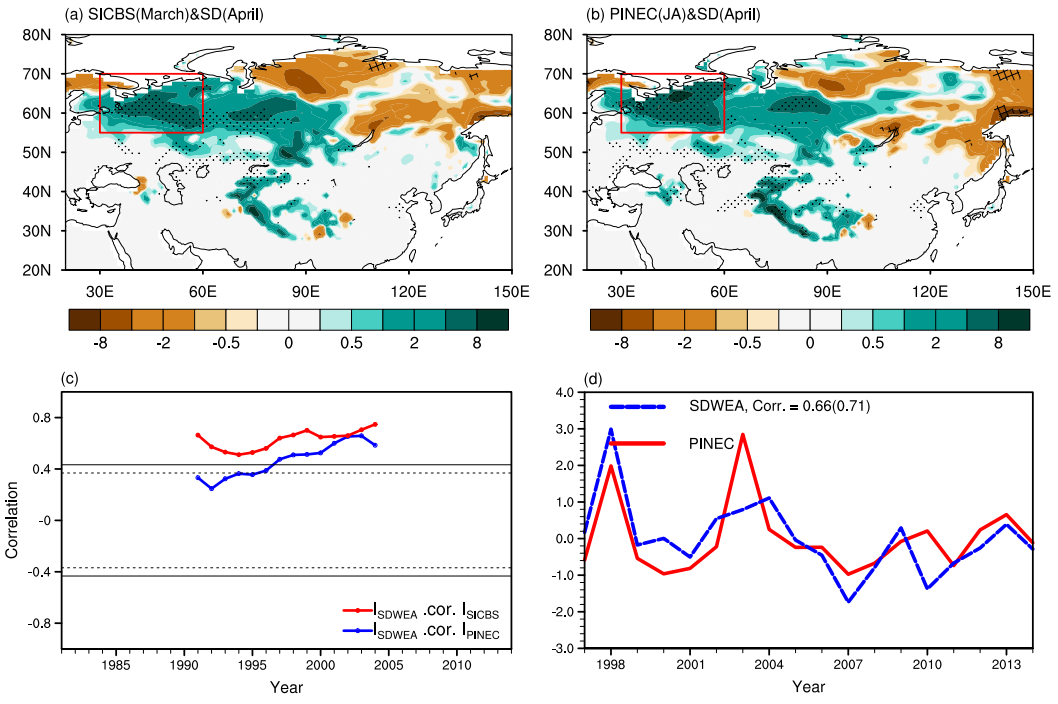

FIG. 8. Regression maps of SD in April with regard to (a) SICBS in March and (b) PINEC in JA. The dotted (hatched) regions represent positive (negative) correlations significant at the 90% confidence level based on the Student's *t* test. (c) The 21-yr sliding correlation coefficient between SDWEA (spatially weighted, averaged over 55°–70°N, 30°–60°E) and PI (blue line), as well as SDWEA and SICBS (red line). The results are based on the detrended series during 1979–2014, and the dashed (solid) horizontal line represents correlations significant at the 95% (99%) confidence level based on the Student's *t* test. (d) Time series of PI in JA (red) and SDWEA in April (blue) during 1997–2014 for standardized results, and the value in the parentheses represents their corresponding values for the detrended series.

favors upward motion and a cyclonic center over the polar region (Fig. S6b). To examine how the SICBS and SDWEA play important roles in the hot droughts over NEC after 1996/97, we further regress the SICBS in March and SDWEA in April and atmospheric circulations in JA during 1997–2016 (Fig. 11). Similar to Fig. 3, we also multiply −1 by SICBS and SDWEA in this case. Influenced by the decreased SICBS in March and SDWEA in April, there is an anomalous cyclonic center over polar region and an anomalous anticyclonic center over NEC (Figs. 11c,d). As a result, the positive POL pattern is evident, accompanied with a wavelike train propagating from the Barents Sea and western Eurasia to NEC. Besides, the anomalous anticyclonic wind centers over NEC are identified (Figs. 11a,b,e,f), accounting for the precipitation deficiencies over NEC. In addition, uniform quasi-barotropic downward motion (Figs. 11g,h) is also evident over NEC, resulting in adiabatic heating and hot events over that region. These regression patterns are quite similar to Fig. 3 and the regression results of PINEC during 1997–2016 (Fig. S7 in the supplemental material).

In addition to the influences of SICBS and SDWEA on summer atmospheric circulations, the decrease of SDWEA in April also shows a close relationship to the anomalous northerly and westerly wind (Figs. S8a,b in the supplemental material) as well as the anomalous downward motion (Fig. S8c) over YRNC and NEC in MJ. These anomalous atmospheric circulations in MJ contribute to insufficient moisture accumulation and dry soil over YRNC (Fig. 10c), which is further linked to less precipitation over NEC in JA according to previous studies.

Subsequently, the positive POL pattern in JA can provide a favorable environment for summer hot drought over NEC (Fig. 5), and it will be more severe under the dry soil condition over NEC in JA. Results indicate that the decline of SICBS in March and the decreased SDWEA in April have close connections to the positive POL pattern (Fig. 11) and dry soil (Figs. 10b,d) over NEC in JA, which are further linked to summer hot droughts over NEC. As demonstrated in Fig. 9, all of these three factors (the decline of SICBS in March, decreased SDWEA in April, and dry SMNEC

Unauthenticated | Downloaded 08/04/22 06:29 PM UTC

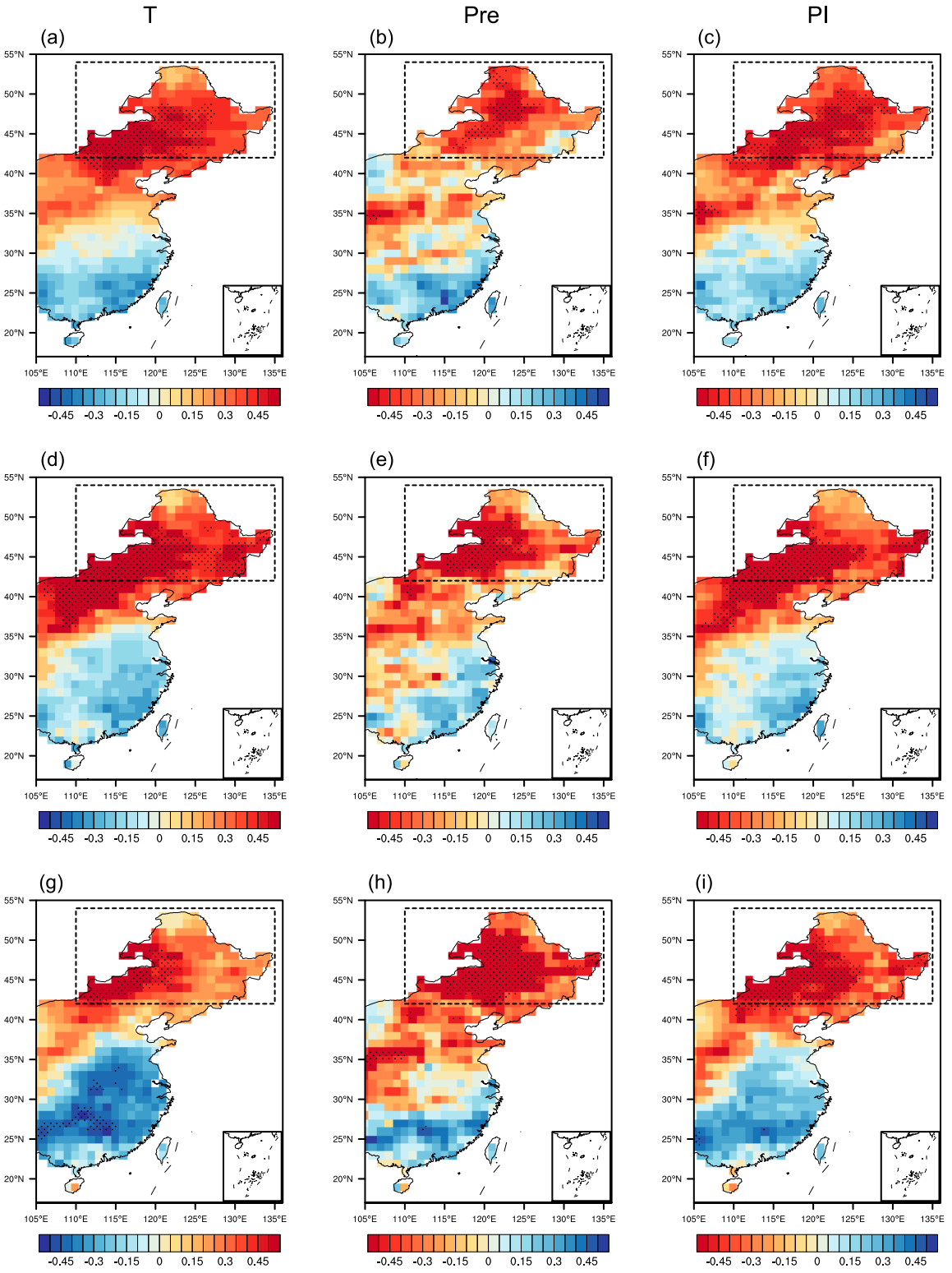

FIG. 9. Regression maps of (left) temperature, (middle) precipitation, and (right) PI in JA with regard to (a)–(c) SICBS in March, (d)–(f) SDWEA in April, and (g)–(i) SMNEC (spatially weighted) in JA. The results are based on the detrended series during 1997–2016, and the dotted regions indicate the regression coefficient significant at the 90% confidence level based on the Student's *t* test. Here, SICBS, SDWEA, and SMNEC are multiplied by −1.

Unauthenticated | Downloaded 08/04/22 06:29 PM UTC

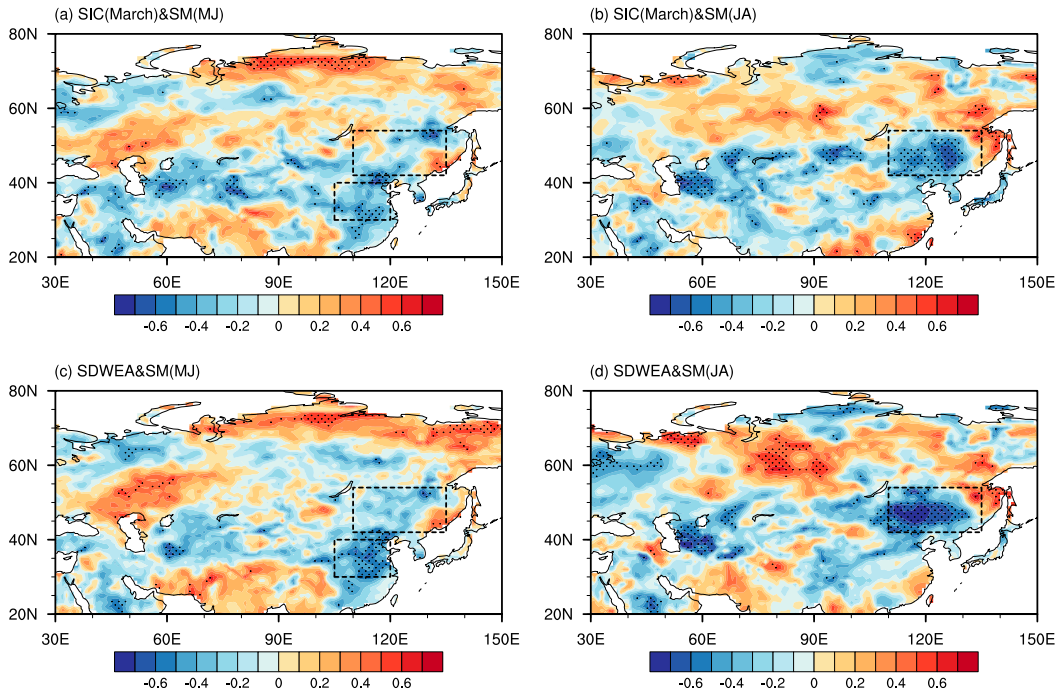

FIG. 10. Regression maps of soil moisture in (a),(c) MJ and (b),(d) JA during 1997–2016 with regard to (top) SICBS in March and (bottom) SDWEA in April. The results are based on detrended and standardized series, and the dotted regions indicate the regression coefficient significant at the 90% confidence level based on the Student's t test. Here, SICBS and SDWEA are multiplied by -1.

in JA) present significant influences on summer hot droughts over NEC (Fig. 9c,f,i) accompanied with high temperature (Fig. 9a,d,g) and less precipitation (Fig. 9b,e,h). In addition to these direct influences of summer POL pattern and summer soil moisture over NEC, soil moisture over YRNC in MJ also serves as the linkage between the SDWEA in April and the hot drought events over NEC in JA.

d. Causality validation by large ensemble model CESM-LE

The possible causality between the decreased SICBS in March or SDWEA in April and hot droughts in JA over NEC has been discussed in the above analyses. Here, the large ensemble simulations from the CESM-LE model are used to further explore whether these relationships can be seen by the model. For convenient comparison with observational and reanalysis results, all of the variables from CESM-LE spanning from 1997 to 2016 are analyzed, with data during 1997–2005 from the historical simulation and during 2006–16 from the RCP8.5 scenario.

We are wondering whether the relationship between SICBS in March and hot droughts over NEC in JA exists in the individual models of CESM-LE. Accompanied by the decreased SICBS in March, about two-thirds of the 35 models present a positive temperature center, negative precipitation center, and negative PI center over NEC in JA (figures not shown). This result suggests that most of the CESM-LE members can reproduce the proposed relationship between SICBS and hot droughts over NEC. To reduce uncertainty from the internal variability, we select the lowest and highest five years for each member and construct the composite maps based on all available members.

First, the composite differences of SIC in March between five low and five high SICBS years during 1997–2016 are investigated based on 35 ensembles of CESM-LE (Fig. 12a). There is about a 10% decline of SIC over the Barents Sea in low years in comparison to high SICBS years. Then the decline of SIC in March favors decreased snow depth over WEA in April (Fig. 12b), which is in good accordance with the observed results (Fig. 8a). Similarly, the possible links between SICBS in March or SDWEA in April and SMNEC in JA are also well reproduced by the model. As seen in Figs. 12c,d, the decline of SICBS in March and decreased SDWEA in April would result in dry soil over NEC in JA, well resembling the observed results (Figs. 10b,d). Besides, the decreased SDWEA in April also favors dry soil over YRNC in MJ.

In terms of the corresponding atmospheric circulations with regard to SICBS in March and SDWEA in

Unauthenticated | Downloaded 08/04/22 06:29 PM UTC

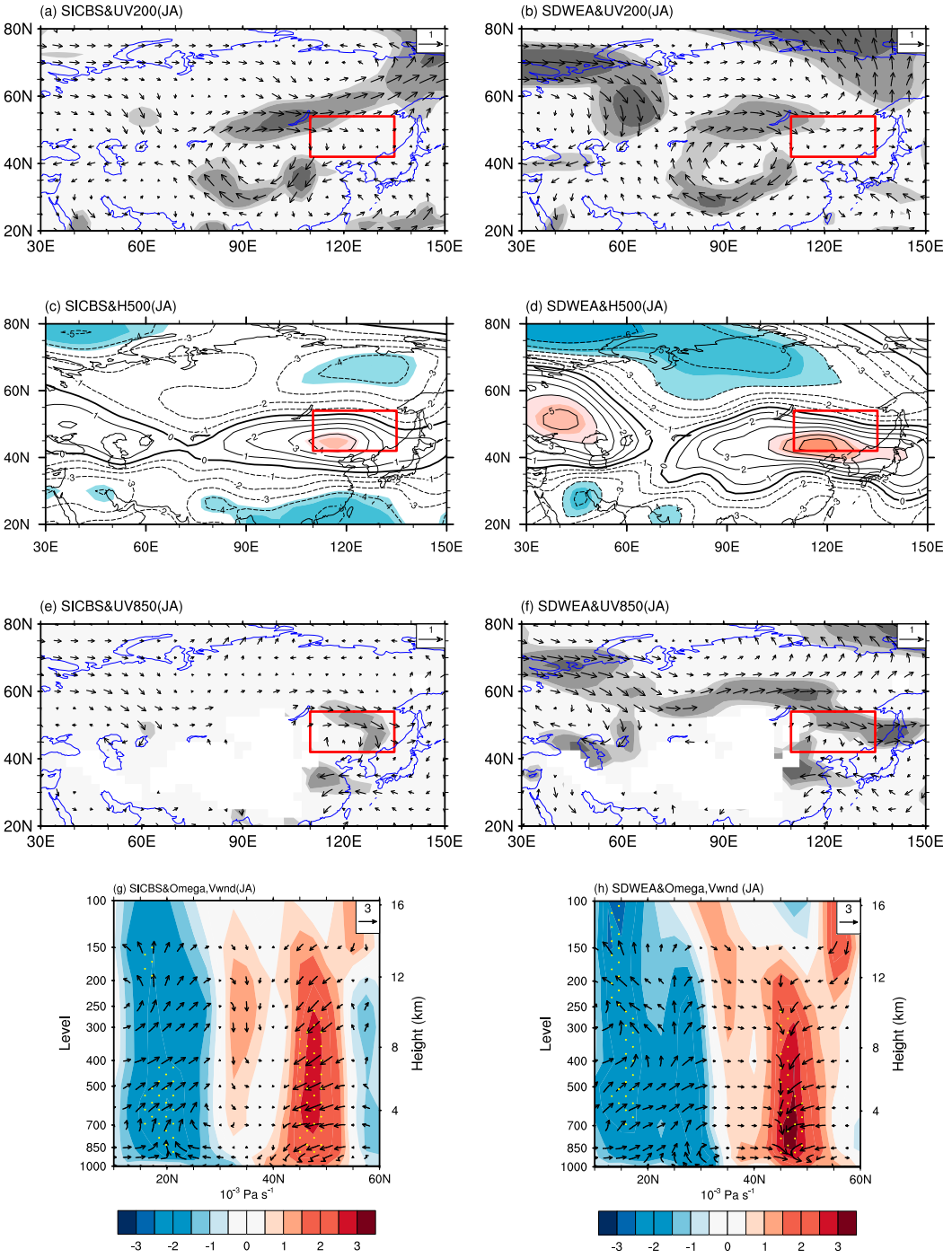

FIG. 11. Regression maps of the circulations in JA with regard to (left) SICBS in March and (right) SDWEA in April during 1997–2016: (a),(b) 200-hPa wind, (c),(d) 500-hPa geopotential height, (e),(f) 850-hPa wind, and (g),(h) vertical–horizontal cross section averaged along 115°–135°E for vertical wind. Results are based on detrended and standardized series. Shading from light to dark in (a)–(f) indicate the regression coefficient significant at the 90%, 95%, and 99% confidence levels based on the Student's t test. The color shading in (g),(h) indicate ω anomalies, and the dotted regions indicate the regression coefficient significant at the 90% confidence level based on the Student's t test. Here, SICBS and SDWEA are multiplied by −1.

Unauthenticated | Downloaded 08/04/22 06:29 PM UTC

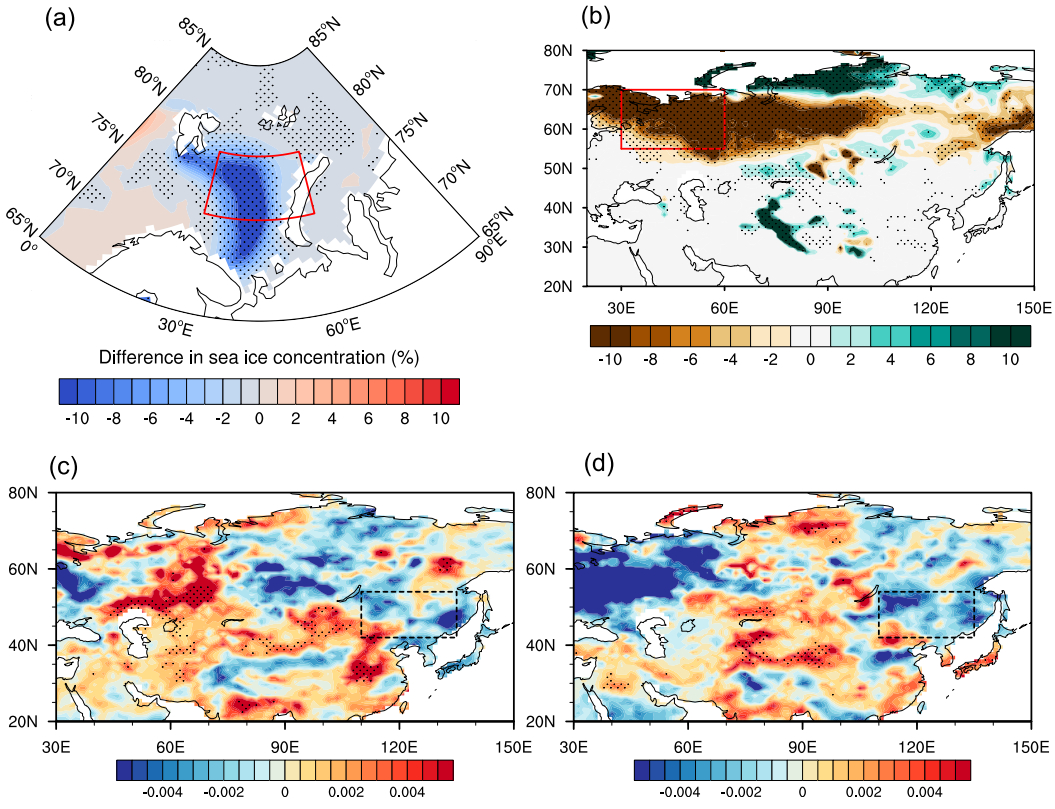

FIG. 12. Composite differences of (a) SIC in March between five low and high SICBS years during 1997–2016 (%) and (b) SD in April between five low and high SICBS years during 1997–2016 (mm). Composite differences of soil moisture in JA between five low and high years of (c) SICBS and (d) SDWEA during 1997–2016 ($mm^3\,mm^{-3}$). Results are based on 35 ensembles of CESM-LE, and the dotted regions indicate the composite differences are significant at the 90% confidence level based on the Student's *t* test.

April, Fig. 13 shows the composite differences for wind at 200 and 850 hPa, respectively. Generally, decreased SDWEA in April results in anomalous northerly wind over NEC and YRNC (Figs. 13a,b) in MJ, thus inducing insufficient moisture concentration over YRNC, which shows much similarity to that from Fig. S8. Similar to Fig. 11, results from CESM-LE indicate that the decreased SICBS in March and decreased SDWEA in April also account for the positive POL patterns (figures not shown) in JA. The anomalous positive POL pattern favors a wavelike train propagating from the Barents Sea to WEA and onto NEC, thus leading to anomalous northeasterly wind at 200 hPa (Figs. 13c,e) and anticyclonic center at 850 hPa (Figs. 13d,f) over NEC. These anomalous atmospheric circulations from MJ to JA contribute to the dry soil over YRNC in MJ and the dry soil over NEC in JA (Figs. 12c,d). Influenced by the dry soil moisture condition and the anomalous atmospheric circulations, we also witness the occurrence of hot droughts (Fig. S9c in the supplemental material) over NEC in JA, accompanied with high SAT (Fig. S9a) and low precipitation (Fig. S9b). Consistent with the observed results, the linkages between the decline of SICBS in March or decreased SDWEA in April and the hot droughts over NEC in JA also exist in CESM-LE. Meanwhile, the corresponding physical mechanisms concerning the modulation of POL pattern and soil moisture are also well verified by models. Since results from CESM-LE capture major features and general physical processes, the decreased Barents Sea ice in March might have been one of the contributing drivers for summer hot droughts over NEC.

e. Validation by sensitivity experiments of CAM4

To provide more robust evidence for the relationship between SICBS in March and hot droughts over NEC, we also conduct numerical experiments to examine the proposed physical processes. Here, we use the Community Atmosphere Model, version 4 (CAM4), to carry out two numerical experiments, including a control experiment and a sensitivity experiment. The CAM4 has a finite volume grid of 1.9° × 2.5° with 26 hybrid sigma–pressure levels. In the control run, the climatological

Unauthenticated | Downloaded 08/04/22 06:29 PM UTC

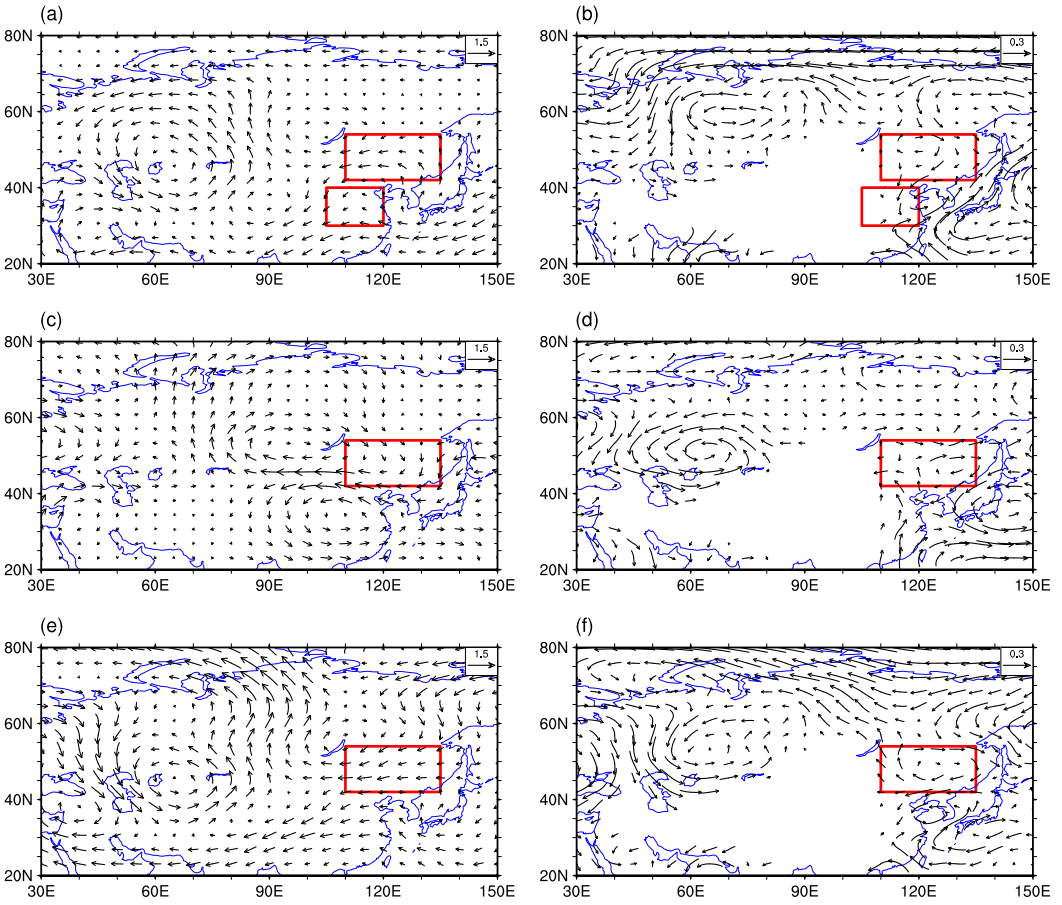

FIG. 13. Composite differences of (a) 200- and (b) 850-hPa wind (m s^{-1}) in MJ between five low and high SDWEA years during 1997–2016. (c),(d) As in (a),(b), but for the differences in JA between low and high SICBS years. (e),(f) As in (c),(d), but for the differences in JA between low and high SDWEA years. Results are based on 35 ensembles of CESM-LE.

monthly means of SST and SIC during 1981–2010 are prescribed as the boundary condition, and the other external variables are fixed. In the sensitivity run, the boundary condition of SIC in March is set as the boundary condition in the control run plus the anomalous lowest SIC in March during 1986–2015 and other months are prescribed as the climatological condition, and the boundary condition of SST is set to −1.8°C where SIC = 0. The control run and sensitivity run are both repeated 40 times, with slight disturbance in initial conditions, integrated from 1 March to 31 August. Then we use the differences between sensitivity experiments and control runs to find the lagged responses to the decreased SICBS in March.

Figure 14 displays the simulated differences between the sensitivity and control experiments with regard to the decrease of SICBS in March based on 40 ensembles of CAM4. To show consistency of different ensembles, we dotted areas where more than 50% of the 40 ensembles share the same sign as the multimodel ensemble mean (MME). The key regions with high consistency are also significant based on the Student's *t* test (see Fig. S10 in the supplemental material). Generally, the decrease of SICBS in March (Fig. 14a) will result in the decline of snow depth over western Eurasia in April (Fig. 14b). It further leads to dry soil over from the Yangtze River valley to northern China in MJ (Fig. 14c) and dry soil over NEC in JA (Fig. 14d). Accompanied with these responses, the lagged responses in atmospheric circulation anomalies are also evident. For example, the geopotential height at 500 hPa is characterized by a positive POL pattern (Fig. 14e), and there is an anomalous anticyclonic center over NEC at 850 hPa (Fig. 14f), which provides an unfavorable environment for moisture accumulation over NEC. Because of the combined influences, warm temperature (Fig. S11a) and less precipitation (Fig. S11b) prevail over most regions of NEC in JA. All

Unauthenticated | Downloaded 08/04/22 06:29 PM UTC

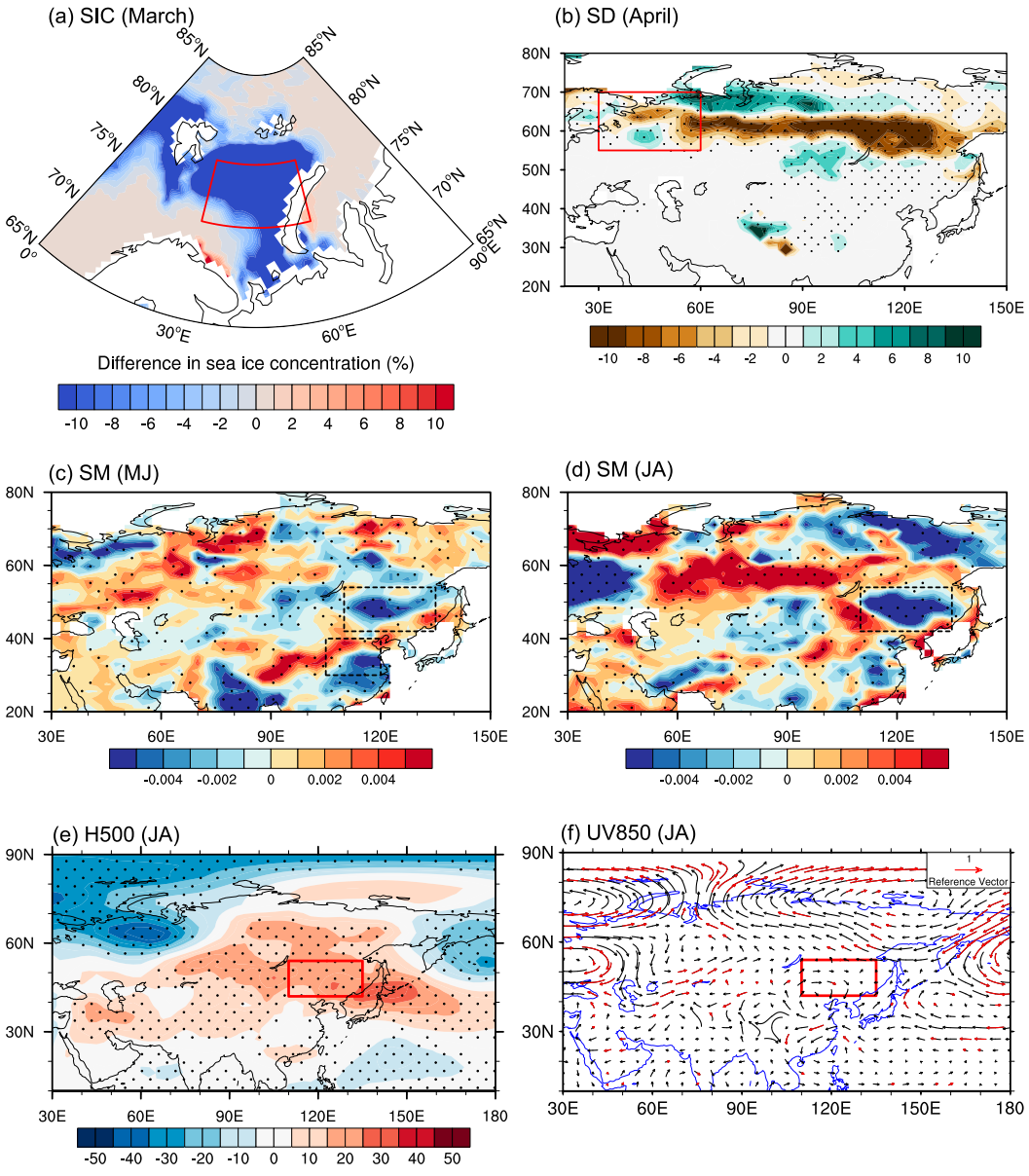

FIG. 14. The composite differences of (a) sea ice concentration in March (%), (b) SD in April (units: mm), (c) soil moisture in MJ ($mm^3\ mm^{-3}$), (d) soil moisture in JA ($mm^3\ mm^{-3}$), (e) geopotential height at 500 hPa in JA (gpm), and (f) 850-hPa wind ($m\ s^{-1}$) in JA between the sensitivity and control experiments based on 40 ensembles of CAM4. The black dotted areas in (b)–(e) and the red arrows in (f) indicate that more than 50% of the 40 ensembles share the same sign as the MME.

of these responses well resemble the observations and CESM-LE, further verifying the proposed linkages.

5. Discussion and conclusions

In this study, we identified the most severe hot drought event over NEC, which occurred in 2016, and we explored its prominent features and possible mechanisms using the multivariate survival method. A hot drought event over NEC is characterized by a positive POL pattern, which is accompanied by an anomalous anticyclonic wind center, a positive geopotential height anomaly, and an obvious descending motion centered over NEC, resulting in less moisture accumulation and high temperature. Clearly, the anomalous atmospheric circulation patterns in 2016 were quite similar to the regressed patterns onto PINEC, which provided a beneficial background for

Unauthenticated | Downloaded 08/04/22 06:29 PM UTC

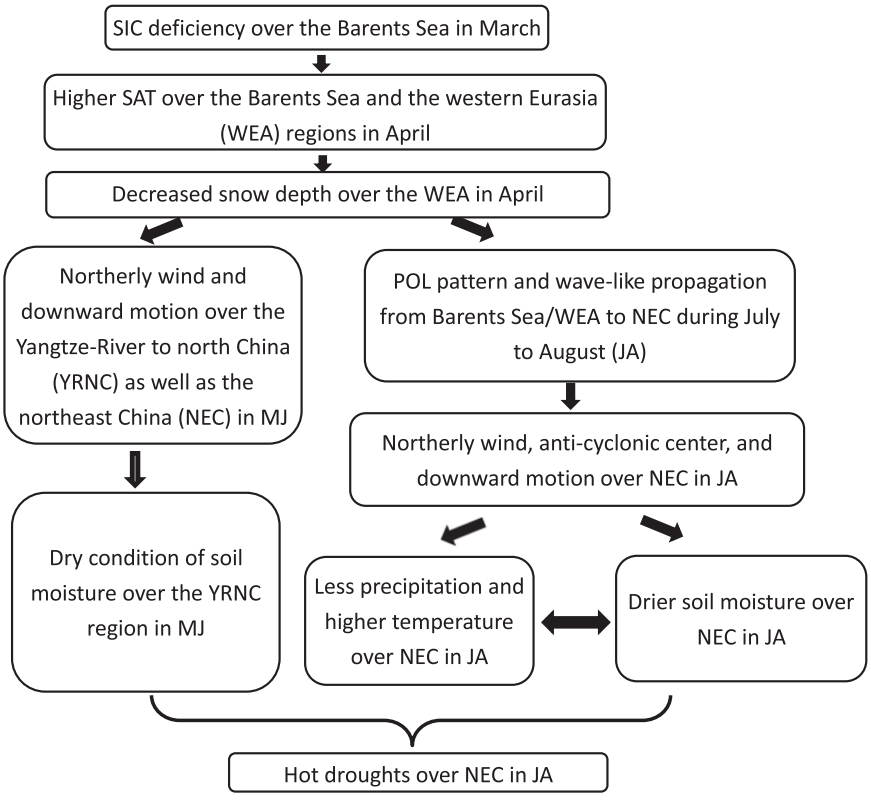

FIG. 15. Schematic diagram illustrating the mechanisms for hot droughts during JA over NEC.

the occurrence of the hot drought event over NEC in that year.

Results indicate that the SICBS in March can partially regulate summer hot droughts over NEC after 1997, and the associated possible physical mechanisms are illustrated in Fig. 15. Clearly, the SIC decline over the Barents Sea in March can influence anomalous adiabatic heating over WEA, thus leading to decline of snow depth in April (Fig. 8a). On the one hand, the decrease of SDWEA might exert influence on atmospheric circulations (Fig. S8) and result in dry soil conditions over YRNC in MJ (Fig. 10c), further leading to the deficiency of precipitation over NEC in JA (Zhang and Zuo 2011). On the other hand, the decline of SICBS in March and SDWEA in April affects the atmospheric circulations in JA, inducing anomalous positive POL pattern in summer (Fig. 11). The anomalous positive POL pattern is accompanied with a wavelike train propagating from the Barents Sea and western Eurasia to NEC (Fig. 11), which favors northerly wind (Figs. 11a,c), anticyclonic geopotential center (Figs. 11c–f), and downward motion (Figs. 11g,h) over NEC, thus leading to drier soil (Figs. 10b,d), higher SAT (Figs. 9a,d,g), and insufficient moisture concentration (Figs. 9b,e,h) over NEC, which can finally influence hot drought events over the region (Figs. 9c,f,i). All of these physical processes have been well confirmed by the large ensemble simulations of the model of CESM-LE and the numerical experiments that based on CAM4.

However, it is worth noting that SICBS in March is not the only factor to influence hot drought events over NEC. Generally, other factors such as the EASM (Sun et al. 2007, 2017), NAO (Sun and Wang 2012), ENSO events (Sun et al. 2004; Dai 2013; X. Li et al. 2015), and so on could also exert influence on interannual variations of precipitation and temperature over NEC. Therefore, the variability in SICBS in March might be one of the potential predictors for the summer hot drought occurrences over NEC. Snow depth and soil moisture generally serve as the linking bridges between SICBS in April and PINEC in JA. In addition, the SIC over the Barents Sea in 2016 was the second lowest year, which also supports our conclusion.

In this study, an increased interannual relationship between SICBS and PINEC is observed after 1996/97, accompanied by an enhanced relationship between SDWEA and PINEC. Hot droughts over NEC also experienced an interdecadal increase in the mid-1990s, resembling the shift of the Atlantic multidecadal oscillation (AMO) variations (Sutton and Dong 2012).

Unauthenticated | Downloaded 08/04/22 06:29 PM UTC

Previous studies have indicated that SIC is intrinsically linked to the AMO (Miles et al. 2014), and evidence indicates that the positive AMO since the 1990s might have caused rapid warming over the North Atlantic, bringing warm water to the Barents Sea and contributing to SIC decline (Day et al. 2012; Fan et al. 2018). Based on these arguments, Screen (2013) has suggested that changes in AMO, sea ice, and precipitation over northern Europe could be interconnected, a theory that shares the common features with this research. In addition, Qian et al. (2014) verified the increasing influence of the AMO on the decadal variations in summer droughts in eastern China. We also find that the decadal variations in the AMO and PI over NEC are highly correlated, with a correlation coefficient of −0.996. Furthermore, the correlation coefficient between the AMO and SICBS is −0.703 and is 0.749 between SICBS and PI. We also noticed that the interdecadal variations of the AMO, PI, and SICBS that occurred around 1996/97 correspond well to the abrupt decrease of PINEC and its enhanced relationship with SICBS. Therefore, the shift of the AMO that occurred in the 1990s might partially account for the increased relationship between SICBS and PINEC after 1996/97. Further analyses relating to these decadal shifts are still needed and will be the focus of future research.

Additionally, in the near future (corresponding to the positive AMO phase), results suggest that a relationship between SICBS and hot droughts might also exist. The decreased SICBS in March will result in decline of snow depth over the western Eurasia in April, accompanied with soil reduction averaged over NEC in JA. Besides, there will be anomalous northerly wind at 850 hPa and an anomalous anticyclonic center at 200 hPa over NEC in JA, which is unfavorable for moisture accumulation. Influenced by these anomalies in atmosphere and soil moisture, we will witness high temperature and low precipitation over NEC, thus leading to hot droughts over this region (figures not shown). Consequently, the Barents Sea ice decline in spring might also enhance summer hot droughts over NEC in the future, and variations of SICBS in March might be a potential predictor for the summer hot drought occurrences over NEC.

Acknowledgments. This research was jointly supported by the National Key Research and Development Program of China (Grant 2016YFA0600701), the Strategic Priority Research Program of the Chinese Academy of Sciences (Grant XDA19070201), External Cooperation Program of BIC, Chinese Academy of Sciences (Grant 134111KYSB20150016), the National Natural Science Foundation of China (Grant 41421004), and the CAS–PKU Joint Research Program.

REFERENCES

AghaKouchak, A., L. Cheng, O. Mazdiyasni, and A. Farahmand, 2014: Global warming and changes in risk of concurrent climate extremes: Insights from the 2014 California drought. *Geophys. Res. Lett.*, **41**, 8847–8852, https://doi.org/10.1002/2014GL062308.

Balsamo, G., and Coauthors, 2015: ERA-Interim/Land: A global land surface reanalysis data set. *Hydrol. Earth Syst. Sci.*, **19**, 389–407, https://doi.org/10.5194/hess-19-389-2015.

Barnes, E. A., and J. A. Screen, 2015: The impact of Arctic warming on the midlatitude jet-stream: Can it? Has it? Will it? *Wiley Interdiscip. Rev.: Climate Change*, **6**, 277–286, https://doi.org/10.1002/wcc.337.

Barnett, T. P., L. Dümenil, U. Schlese, E. Roeckner, and M. Latif, 1989: The effect of Eurasian snow cover on regional and global climate variations. *J. Atmos. Sci.*, **46**, 661–685, https://doi.org/10.1175/1520-0469(1989)046<0661:TEOESC>2.0.CO;2.

Chen, H., and J. Sun, 2015a: Changes in drought characteristics over China using the standardized precipitation evapotranspiration index. *J. Climate*, **28**, 5430–5447, https://doi.org/10.1175/JCLI-D-14-00707.1.

——, and ——, 2015b: Drought response to air temperature change over China on the centennial scale. *Atmos. Oceanic Sci. Lett.*, **8**, 113–119, https://doi.org/10.3878/AOSL20140089.

——, and ——, 2017a: Characterizing present and future drought changes over eastern China. *Int. J. Climatol.*, **17**, 138–156, https://doi.org/10.1002/joc.4987.

——, and ——, 2017b: Anthropogenic warming has caused hot droughts more frequently in China. *J. Hydrol.*, **544**, 306–318, https://doi.org/10.1016/j.jhydrol.2016.11.044.

Cheng, L., M. Hoerling, A. AghaKouchak, B. Livneh, X. Quan, and J. Eischeid, 2016: How has human-induced climate change affected California drought risk? *J. Climate*, **29**, 111–120, https://doi.org/10.1175/JCLI-D-15-0260.1.

Dai, A., 2013: Increasing drought under global warming in observations and models. *Nat. Climate Change*, **3**, 52–58, https://doi.org/10.1038/nclimate1633.

Day, J. J., J. C. Hargreaves, J. D. Annan, and A. Abe-Ouchi, 2012: Sources of multi-decadal variability in Arctic sea ice extent. *Environ. Res. Lett.*, **7**, 034011, https://doi.org/10.1088/1748-9326/7/3/034011.

De Michele, C., G. Salvadori, M. Canossi, A. Petaccia, and R. Rosso, 2005: Bivariate statistical approach to check adequacy of dam spillway. *J. Hydrol. Eng.*, **10**, 50–57, https://doi.org/10.1061/(ASCE)1084-0699(2005)10:1(50).

Ding, Y., Y. Sun, Z. Wang, Y. Zhu, and Y. Song, 2009: Inter-decadal variation of the summer precipitation in China and its association with decreasing Asian summer monsoon. Part II: Possible causes. *Int. J. Climatol.*, **29**, 1926–1944, https://doi.org/10.1002/joc.1759.

Durante, F., and G. Salvadori, 2010: On the construction of multivariate extreme value models via copulas. *Environmetrics*, **21**, 143–161, https://doi.org/10.1002/env.988.

Fan, K., Z. Xie, H. Wang, Z. Xu, and J. Liu, 2018: Frequency of spring dust weather in North China linked to sea ice variability in the Barents Sea. *Climate Dyn.*, https://doi.org/10.1007/s00382-016-3515-7, in press.

Fu, C., and Z. Zeng, 2005: Correlations between North Atlantic Oscillation index in winter and eastern China flood/drought index in summer in the last 530 years. *Sci. Bull.*, **50**, 2505–2516, https://doi.org/10.1007/BF03183642.

Unauthenticated | Downloaded 08/04/22 06:29 PM UTC

Gao, T., J. Yu, and H. Paek, 2017: Impacts of four Northern-Hemisphere teleconnection patterns on atmospheric circulations over Eurasia and the Pacific. *Theor. Appl. Climatol.*, **129**, 815–831, https://doi.org/10.1007/s00704-016-1801-2.

Gao, Y., and Coauthors, 2015: Arctic sea ice and Eurasian climate: A review. *Adv. Atmos. Sci.*, **32**, 92–114, https://doi.org/10.1007/s00376-014-0009-6.

Guo, D., Y. Gao, I. Bethke, D. Gong, O. M. Johannessen, and H. Wang, 2014: Mechanism on how the spring Arctic sea ice impacts the East Asian summer monsoon. *Theor. Appl. Climatol.*, **115**, 107–119, https://doi.org/10.1007/s00704-013-0872-6.

Han, T., H. Chen, and H. Wang, 2015: Recent changes in summer precipitation in northeast China and the background circulation. *Int. J. Climatol.*, **35**, 4210–4219, https://doi.org/10.1002/joc.4280.

——, H. Wang, and J. Sun, 2017: Strengthened relationship between eastern ENSO and summer precipitation over northeastern China. *J. Climate*, **30**, 4497–4512, https://doi.org/10.1175/JCLI-D-16-0551.1.

He, S., Y. Gao, T. Furevik, H. Wang, and F. Li, 2018: Teleconnection between sea ice in the Barents Sea in June and the Silk Road, Pacific–Japan and East Asian rainfall patterns in August. *Adv. Atmos. Sci.*, **35**, 52–64, https://doi.org/10.1007/s00376-017-7029-y.

Inoue, J., M. E. Hori, and K. Takaya, 2012: The role of Barents Sea ice in the wintertime cyclone track and emergence of a warm-Arctic cold-Siberian anomaly. *J. Climate*, **25**, 2561–2568, https://doi.org/10.1175/JCLI-D-11-00449.1.

Kalnay, E., and Coauthors, 1996: The NCEP/NCAR 40-Year Reanalysis Project. *Bull. Amer. Meteor. Soc.*, **77**, 437–471, https://doi.org/10.1175/1520-0477(1996)077<0437:TNYRP>2.0.CO;2.

Kay, J. E., and Coauthors, 2015: The Community Earth System Model (CESM) Large Ensemble Project: A community resource for studying climate change in the presence of internal climate variability. *Bull. Amer. Meteor. Soc.*, **96**, 1333–1349, https://doi.org/10.1175/BAMS-D-13-00255.1.

Kelleher, M., and J. Screen, 2017: Atmospheric precursors of and response to anomalous Arctic sea ice in CMIP5 models. *Adv. Atmos. Sci.*, **35**, 27–37, https://doi.org/10.1007/s00376-017-7039-9.

Kim, B.-M., S.-W. Son, S.-K. Min, J.-H. Jeong, S.-J. Kim, X. D. Zhang, T. Shim, and J.-H. Yoon, 2014: Weakening of the stratospheric polar vortex by Arctic sea-ice loss. *Nat. Commun.*, **5**, 4646, https://doi.org/10.1038/ncomms5646.

Li, F., and H. Wang, 2013: Relationship between Bering Sea ice cover and East Asian winter monsoon year-to-year variations. *Adv. Atmos. Sci.*, **30**, 48–56, https://doi.org/10.1007/s00376-012-2071-2.

——, and ——, 2014: Autumn Eurasian snow depth, autumn Arctic sea ice cover and East Asian winter monsoon. *Int. J. Climatol.*, **34**, 3616–3625, https://doi.org/10.1002/joc.3936.

——, ——, and Y. Gao, 2015: Change in sea ice cover is responsible for non-uniform variation in winter temperature over East Asia. *Atmos. Oceanic Sci. Lett.*, **8**, 376–382, https://doi.org/10.3878/AOSL20150039.

Li, X., W. Zhou, and Y. Chen, 2015: Assessment of regional drought trend and risk over China: A drought climate division perspective. *J. Climate*, **28**, 7025–7037, https://doi.org/10.1175/JCLI-D-14-00403.1.

Li, Y., H. Xu, and D. Liu, 2011: Features of the extremely severe drought in the east of southwest China and anomalies of atmospheric circulation in summer 2006. *Acta Meteor. Sin.*, **25**, 176–187, https://doi.org/10.1007/s13351-011-0025-8.

Liang, L., L. Li, and L. Qiang, 2011: Precipitation variability in northeast China from 1961 to 2008. *J. Hydrol.*, **404**, 67–76, https://doi.org/10.1016/j.jhydrol.2011.04.020.

Liu, J., J. A. Curry, H. Wang, M. Song, and R. M. Horton, 2012: Impact of declining Arctic sea ice on winter snowfall. *Proc. Natl. Acad. Sci. USA*, **109**, 4074–4079, https://doi.org/10.1073/pnas.1114910109.

Liu, X., S. Wang, Y. Zhou, F. Wang, W. Li, and W. Liu, 2015: Regionalization and spatiotemporal variation of drought in China based on Standardized Precipitation Evapotranspiration Index (1961–2013). *Adv. Meteor.*, **2015**, 950262, https://doi.org/10.1155/2015/950262.

Miles, M. W., D. V. Divine, T. Furevik, E. Jansen, M. Moros, and A. E. J. Ogilvie, 2014: A signal of persistent Atlantic multidecadal variability in Arctic sea ice. *Geophys. Res. Lett.*, **41**, 463–469, https://doi.org/10.1002/2013GL058084.

Petoukhov, V., and V. A. Semenov, 2010: A link between reduced Barents-Kara sea ice and cold winter extremes over northern continents. *J. Geophys. Res.*, **115**, D21111, https://doi.org/10.1029/2009JD013568.

Qian, C., J. Yu, and G. Chen, 2014: Decadal summer drought frequency in China: The increasing influence of the Atlantic Multi-decadal Oscillation. *Environ. Res. Lett.*, **9**, 124004, https://doi.org/10.1088/1748-9326/9/12/124004.

Rayner, N. A., D. E. Parker, E. B. Horton, C. K. Folland, L. V. Alexander, D. P. Rowell, E. C. Kent, and A. Kaplan, 2003: Global analyses of sea surface temperature, sea ice, and night marine air temperature since the late nineteenth century. *J. Geophys. Res.*, **108**, 4407, https://doi.org/10.1029/2002JD002670.

Salvadori, G., and C. De Michele, 2010: Multivariate multiparameter extreme value models and return periods: A copula approach. *Water Resour. Res.*, **46**, W10501, https://doi.org/10.1029/2009WR009040.

——, ——, and F. Durante, 2011: On the return period and design in a multivariate framework. *Hydrol. Earth Syst. Sci.*, **15**, 3293–3305, https://doi.org/10.5194/hess-15-3293-2011.

——, F. Durante, and C. De Michele, 2013: Multivariate return period calculation via survival functions. *Water Resour. Res.*, **49**, 2308–2311, https://doi.org/10.1002/wrcr.20204.

Screen, J. A., 2013: Influence of Arctic sea ice on European summer precipitation. *Environ. Res. Lett.*, **8**, 044015, https://doi.org/10.1088/1748-9326/8/4/044015.

——, I. Simmonds, C. Deser, and R. Tomas, 2013: The atmospheric response to three decades of observed Arctic sea ice loss. *J. Climate*, **26**, 1230–1248, https://doi.org/10.1175/JCLI-D-12-00063.1.

——, C. Deser, I. Simmonds, and R. Tomas, 2014: Atmospheric impacts of Arctic sea-ice loss, 1979–2009: Separating forced change from atmospheric internal variability. *Climate Dyn.*, **43**, 333–344, https://doi.org/10.1007/s00382-013-1830-9.

Seviour, W. J. M., 2017: Weakening and shift of the Arctic stratospheric polar vortex: Internal variability or forced response? *Geophys. Res. Lett.*, **44**, 3365–3373, https://doi.org/10.1002/2017GL073071.

Sun, J., and H. Wang, 2012: Changes of the connection between the summer North Atlantic Oscillation and the East Asian summer rainfall. *J. Geophys. Res.*, **117**, D08110, https://doi.org/10.1029/2012JD017482.

Sun, L., B. Shen, G. An, and X. Tang, 2004: A study on the relationship between the summer precipitation in northeast China and the global sea surface temperature anomaly (SSTA) in preceding seasons. *J. Trop. Meteor.*, **10**, 43–52.

——, ——, Z. Gao, B. Sui, S. Wang, G. An, and J. Li, 2007: The Impacts of moisture transport of East Asian monsoon on summer precipitation in northeast China. *Adv. Atmos. Sci.*, **24**, 606–618, https://doi.org/10.1007/s00376-007-0606-8.

Unauthenticated | Downloaded 08/04/22 06:29 PM UTC

——, ——, B. Sui, and B. Huang, 2017: The influences of East Asian monsoon on summer precipitation in northeast China. *Climate Dyn.*, **48**, 1647–1659, https://doi.org/10.1007/s00382-016-3165-9.

Sutton, R. T., and B. Dong, 2012: Atlantic Ocean influence on a shift in European climate in the 1990s. *Nat. Geosci.*, **5**, 788–792, https://doi.org/10.1038/ngeo1595.

Trenberth, K. E., A. Dai, G. van der Schrier, P. D. Jones, J. Barichivich, K. R. Briffa, and J. Sheffield, 2014: Global warming and changes in drought. *Nat. Climate Change*, **4**, 17–22, https://doi.org/10.1038/nclimate2067.

Wang, H., 2001: The weakening of the Asian monsoon circulation after the end of 1970's. *Adv. Atmos. Sci.*, **18**, 376–386, https://doi.org/10.1007/BF02919316.

——, and S. He, 2015: The north China/northeastern Asia severe summer drought in 2014. *J. Climate*, **28**, 6667–6681, https://doi.org/10.1175/JCLI-D-15-0202.1.

——, and H. Chen, 2016: Understanding the recent trend of haze pollution in eastern China: Roles of climate change. *Atmos. Chem. Phys.*, **16**, 4205–4211, https://doi.org/10.5194/acp-16-4205-2016.

——, and Coauthors, 2012: Extreme climate in China: Facts, simulation and projection. *Meteor. Z.*, **21**, 279–304, https://doi.org/10.1127/0941-2948/2012/0330.

——, H. Chen, and J. Liu, 2015: Arctic Sea ice decline intensified haze pollution in eastern China. *Atmos. Oceanic Sci. Lett.*, **8**, 1–9, https://doi.org/10.3878/AOSL20140081.

Wang, L., X. Yuan, Z. Xie, P. Wu, and Y. Li, 2016: Increasing flash droughts over China during the recent global warming hiatus. *Sci. Rep.*, **6**, 30571, https://doi.org/10.1038/srep30571.

Wilks, D. S., 2011: *Statistical Methods in the Atmospheric Sciences*. Academic Press, 676 pp.

Wu, B., R. Huang, and D. Gao, 1999: Effects of variation of winter sea-ice area in Kara and Barents Seas on East Asian winter monsoon. *Acta Meteor. Sin.*, **13**, 141–153, http://www.cmsjournal.net:8080/Jweb_jmr/EN/Y1999/V13/I2/141.

——, J. Su, and R. Zhang, 2011: Effects of autumn–winter Arctic sea ice on winter Siberian high. *Chin. Sci. Bull.*, **56**, 3220–3228, https://doi.org/10.1007/s11434-011-4696-4.

——, R. Zhang, R. D'Arrigo, and J. Su, 2013: On the relationship between winter sea ice and summer atmospheric circulation over Eurasia. *J. Climate*, **26**, 5523–5536, https://doi.org/10.1175/JCLI-D-12-00524.1.

Wu, R., and B. P. Kirtman, 2007: Observed relationship of spring and summer East Asian rainfall with winter and spring Eurasian snow. *J. Climate*, **20**, 1285–1304, https://doi.org/10.1175/JCLI4068.1.

——, G. Liu, and Z. Ping, 2014: Contrasting Eurasian spring and summer climate anomalies associated with western and eastern Eurasian spring snow cover changes. *J. Geophys. Res. Atmos.*, **119**, 7410–7424, https://doi.org/10.1002/2014JD021764.

Xu, Z., K. Fan, and H. Wang, 2017: Role of sea surface temperature anomalies in the tropical Indo-Pacific region in the northeast Asia severe drought in summer 2014: Month-to-month perspective. *Climate Dyn.*, **49**, 1631–1650, https://doi.org/10.1007/s00382-016-3406-y.

Yang, J., D. Gong, W. Wang, M. Hu, and R. Mao, 2012: Extreme drought event of 2009/2010 over southwestern China. *Meteor. Atmos. Phys.*, **115**, 173–184, https://doi.org/10.1007/s00703-011-0172-6.

Yu, M., Q. Li, M. J. Hayes, M. D. Svoboda, and R. R. Heim, 2014: Are droughts becoming more frequent or severe in China based on the Standardized Precipitation Evapotranspiration Index: 1951–2010? *Int. J. Climatol.*, **34**, 545–558, https://doi.org/10.1002/joc.3701.

Zhang, Q., J. Li, V. P. Singh, and C. Xu, 2013: Copula-based spatio-temporal patterns of precipitation extremes in China. *Int. J. Climatol.*, **33**, 1140–1152, https://doi.org/10.1002/joc.3499.

Zhang, R., and Z. Zuo, 2011: Impact of spring soil moisture on surface energy balance and summer monsoon circulation over East Asia and precipitation in east China. *J. Climate*, **24**, 3309–3322, https://doi.org/10.1175/2011JCLI4084.1.

——, R. Zhang, and Z. Zuo, 2016: An overview of wintertime snow cover characteristics over China and the impact of Eurasian snow cover on Chinese climate (in Chinese). *J. Appl. Meteor. Sci.*, **27**, 513–526.

Unauthenticated | Downloaded 08/04/22 06:29 PM UTC